

---

This is an electronic reprint of the original article.  
This reprint may differ from the original in pagination and typographic detail.

Västilä, Kaisa; Järvelä, Juha

**Characterizing natural riparian vegetation for modeling of flow and suspended sediment transport**

*Published in:*  
JOURNAL OF SOILS AND SEDIMENTS

*DOI:*  
[10.1007/s11368-017-1776-3](https://doi.org/10.1007/s11368-017-1776-3)

Published: 01/10/2018

*Document Version*  
Peer reviewed version

*Please cite the original version:*  
Västilä, K., & Järvelä, J. (2018). Characterizing natural riparian vegetation for modeling of flow and suspended sediment transport. *JOURNAL OF SOILS AND SEDIMENTS*, 18(10), 3114-3130.  
<https://doi.org/10.1007/s11368-017-1776-3>

---

This material is protected by copyright and other intellectual property rights, and duplication or sale of all or part of any of the repository collections is not permitted, except that material may be duplicated by you for your research use or educational purposes in electronic or print form. You must obtain permission for any other use. Electronic or print copies may not be offered, whether for sale or otherwise to anyone who is not an authorised user.

# Journal of Soils and Sediments

## Characterizing natural riparian vegetation for modeling of flow and suspended sediment transport --Manuscript Draft--

<b>Manuscript Number:</b>	JSSS-D-16-00811R2	
<b>Full Title:</b>	Characterizing natural riparian vegetation for modeling of flow and suspended sediment transport	
<b>Article Type:</b>	SI: Physical and Ecological Aspects of Mobile Sediments	
<b>Section/Category:</b>	Sediments	
<b>Corresponding Author:</b>	Kaisa Västilä, D.Sc. (Tech.) Aalto University School of Engineering FINLAND	
<b>Corresponding Author Secondary Information:</b>		
<b>Corresponding Author's Institution:</b>	Aalto University School of Engineering	
<b>Corresponding Author's Secondary Institution:</b>		
<b>First Author:</b>	Kaisa Västilä, D.Sc. (Tech.)	
<b>First Author Secondary Information:</b>		
<b>Order of Authors:</b>	Kaisa Västilä, D.Sc. (Tech.) Juha Järvelä, D.Sc. (Tech.)	
<b>Order of Authors Secondary Information:</b>		
<b>Funding Information:</b>	Maa- ja vesitekniikan tuki ry (700693)	Not applicable
<b>Abstract:</b>	<p>Purpose: Riparian vegetation imposes a critical control on the transport and deposition of suspended sediment with important implications on water quality and channel maintenance. This paper contributes 1) to hydraulic and morphological modeling by examining the parameterization of natural riparian vegetation (trees, bushes, and grasses) and 2) to the design and management of environmental channels by determining how the properties of natural floodplain plant stands affect the erosion and deposition of suspended sediment.</p> <p>Materials and methods: Laboratory and field data were employed for enhancing physically solid description of the flow-plant-sediment interactions with a view on practical applicability. A drag force parameterization that takes into account the flexibility-induced reconfiguration and the complex structure of foliated plants was validated for small natural trees under laboratory conditions, while the data from a small vegetated compound channel allowed demonstrating the approaches at the field scale. Based on the field data, we identified three key vegetative factors influencing the net deposition and erosion on the floodplain. The significance of these factors was evaluated for vegetative conditions ranging from almost bare soil to sparse willows and dense grasses. Overall, the investigated conditions covered flexible and rigid vegetation with seasonal differences represented by foliated and leafless states.</p> <p>Results and discussion: The drag and reconfiguration of woody plants were reliably predicted under leafless and foliated conditions. Subsequently, we present a new easy-to-use methodology for predicting vegetative drag and flow resistance. The methodology is based on a physically solid parameterization for five widely used coefficients or terms (Eqs. 2-6), with the necessary parameter values presented for common riparian species. The methodology was coupled with existing approaches at the field scale, revealing that increasing vegetation density and the associated decreasing flow velocity within vegetation significantly increased net deposition. Further, deposition increased with increasing cross-sectional vegetative blockage and decreasing distance from the suspended sediment replenishment point. Thus, longitudinal advection was the most important mechanism supplying fine sediment to</p>	

	<p>the floodplain, but long continuous plant stands limited deposition.</p> <p>Conclusions: The proposed parameterization (Eqs. 2-6) can be readily implemented into existing hydraulic and morphological models to improve the description of natural vegetation compared to the conventional rigid cylinder representation. The approach is advantageous for evaluating e.g. the effects of both natural succession and management interventions on floodplains. Finally, guidance is provided on how floodplain vegetation can be maintained to manage the erosion and deposition of suspended sediment in environmental channel designs.</p>
<b>Response to Reviewers:</b>	Please, see attachment.

1 PHYSICAL AND ECOLOGICAL ASPECTS OF MOBILE SEDIMENTS

2

3 **Characterizing natural riparian vegetation for modeling of flow and suspended sediment**  
4 **transport**

5

6 **Kaisa Västilä<sup>1</sup> • Juha Järvelä<sup>1</sup>**

7

8 <sup>1</sup>Water Engineering, Aalto University School of Engineering, Espoo, Finland

9

10

11 ✉ Kaisa Västilä

12 [kaisa.vastila@aalto.fi](mailto:kaisa.vastila@aalto.fi)

13 *tel. +358 504081390*

14 ORCID: 0000-0002-6034-760X

15

16 **Abstract**

17 *Purpose:* Riparian vegetation imposes a critical control on the transport and deposition of suspended  
18 sediment with important implications on water quality and channel maintenance. This paper contributes  
19 1) to hydraulic and morphological modeling by examining the parameterization of natural riparian  
20 vegetation (trees, bushes, and grasses) and 2) to the design and management of environmental channels  
21 by determining how the properties of natural floodplain plant stands affect the erosion and deposition  
22 of suspended sediment.

23 *Materials and methods:* Laboratory and field data were employed for enhancing physically solid  
24 description of the flow–plant–sediment interactions with a view on practical applicability. A drag force  
25 parameterization that takes into account the flexibility-induced reconfiguration and the complex  
26 structure of foliated plants was validated for small natural trees under laboratory conditions, while the  
27 data from a small vegetated compound channel allowed demonstrating the approaches at the field scale.  
28 Based on the field data, we identified three key vegetative factors influencing the net deposition and  
29 erosion on the floodplain. The significance of these factors was evaluated for vegetative conditions  
30 ranging from almost bare soil to sparse willows and dense grasses. Overall, the investigated conditions  
31 covered flexible and rigid vegetation with seasonal differences represented by foliated and leafless  
32 states.

33 *Results and discussion:* The drag and reconfiguration of woody plants were reliably predicted under  
34 leafless and foliated conditions. Subsequently, we present a new easy-to-use methodology for predicting  
35 vegetative drag and flow resistance. The methodology is based on a physically solid parameterization  
36 for five widely used coefficients or terms (Eqs. 2–6), with the necessary parameter values presented for  
37 common riparian species. The methodology was coupled with existing approaches at the field scale,  
38 revealing that increasing vegetation density and the associated decreasing flow velocity within vegeta-  
39 tion significantly increased net deposition. Further, deposition increased with increasing cross-sectional  
40 vegetative blockage and decreasing distance from the suspended sediment replenishment point. Thus,  
41 longitudinal advection was the most important mechanism supplying fine sediment to the floodplain,  
42 but long continuous plant stands limited deposition.

43 *Conclusions:* The proposed parameterization (Eqs. 2–6) can be readily implemented into existing hy-  
44 draulic and morphological models to improve the description of natural vegetation compared to the  
45 conventional rigid cylinder representation. The approach is advantageous for evaluating e.g. the effects  
46 of both natural succession and management interventions on floodplains. Finally, guidance is provided  
47 on how floodplain vegetation can be maintained to manage the erosion and deposition of suspended  
48 sediment in environmental channel designs.

49 *Keywords:* cohesive sediment, suspended sediment, deposition, vegetation, flow resistance, drag force

50

## 51 1 Introduction

52 Woody and grassy riparian vegetation growing on river banks and floodplains is a vital part of fluvial  
53 ecosystems (e.g. Naiman and Décamps 1997). Accordingly, regulatory norms such as the Water  
54 Framework Directive of the European Union demand improving and preserving the diversity, structure  
55 and ecological functioning of not only aquatic but also riparian zones. Riparian plant stands can exert a  
56 notable control on the seasonal flow resistance and water levels (e.g., Sellin and van Beesten 2004;  
57 Västilä et al. 2016) as well as on erosion, deposition and transport processes of fine sediment (e.g.  
58 Arboleda et al. 2010; Osterkamp et al. 2012; Gurnell 2014). Predicting these vegetative effects is  
59 important e.g. for flood management, agricultural drainage, and stream restoration. Furthermore,  
60 suitable maintenance of riparian vegetation can potentially allow for environmentally friendly  
61 management of sediment transport. Currently, some of the most severe problems in river systems are  
62 related to the excessive, unmanaged transport and deposition of fine sediment (e.g. Owens et al. 2005)  
63 with negative effects on fauna and flora (e.g. Wood and Armitage 1997) and water quality through  
64 substances sorbed on the sediment (e.g. Uusitalo et al. 2000).

65 Riparian vegetation is nowadays an essential element in the management of watercourses. For  
66 instance, soil bioengineering methods using plant materials (e.g., Li and Eddleman 2002; Studer and  
67 Zech 2014) can be combined with conventional technical measures even in highly urbanized or heavily  
68 used rivers for stabilizing the banks, protecting against erosion and providing ecological benefits (e.g.  
69 Li et al. 2006; Fleischer and Soyeaux 2013). Another application is the excavation or lowering of  
70 floodplains as an environmentally preferable alternative to conventional trapezoidal channels for  
71 agricultural drainage (e.g., USDA 2007; Västilä and Järvelä 2011) and flood management in low-energy  
72 environments (e.g., Sellin and van Beesten 2004; Geerling et al. 2008; Villada Arroyave and Crosato  
73 2010). Such compound (or two-stage) channels are designed to have a narrow cross-section below the  
74 floodplain level to ensure that there is no notable net aggradation on the channel bed at low to medium  
75 flows, thus bringing sediment transport closer to a state of dynamic equilibrium compared to aggrading  
76 over-wide cross-sections (e.g. USDA 2007). Two-stage channels enhance water quality through net  
77 retention of suspended sediment (SS), sediment-bound substances and nutrients on the vegetated  
78 floodplain (e.g. Mahl et al. 2015; Västilä et al. 2015, 2016). However, the role and characteristics of  
79 natural riparian plant stands in controlling erosion, storage or release of sediment are little studied under  
80 field conditions (e.g. Osterkamp et al. 2012). Uncertainties associated with the suitable parameterization  
81 of natural plants complicate the usage of sophisticated hydraulic and morphological models for real  
82 vegetated channels (e.g. Vargas-Luna et al. 2015a).

83 The modeling of sediment transport rates and morphological processes is sensitive to the parameter-  
84 ization of roughness (e.g., Zinke et al. 2011; Schuurman et al. 2013; Kasvi et al. 2015). In particular,  
85 Zinke et al. (2011) state that the correct parameterization of vegetation remains one of the most im-  
86 portant factors of uncertainty in morphological modeling. Natural riparian plants are flexible and com-  
87 plex in structure, but they are mostly parameterized as rigid cylinders in hydraulic and morphological

88 models. For shrubs, bushes and trees, the behavior of the woody trunks and branches (herein referred to  
89 as stems) under flow is notably different from that of the more flexible foliage (e.g. Vogel 1994; Kouwen  
90 and Fathi-Moghadam 2000; Västilä and Järvelä 2014). The flexibility enables the different plant parts  
91 to bend and streamline under flow, which is referred to as reconfiguration (e.g. de Langre 2008). As this  
92 reconfiguration decreases the drag forces and flow resistance (e.g. Järvelä 2004; Jalonen and Järvelä  
93 2014, Whittaker et al. 2015), the behavior of both foliated and leafless riparian vegetation notably differs  
94 from that of rigid elements for which the drag force ( $F$ ) and flow velocity ( $u_c$ ) are related as  $F \propto u_c^2$  (see  
95 also Figures 5 and 6 in Aberle and Järvelä 2013; and Figure 21.4 in Aberle and Järvelä 2015). Overall,  
96 the parameterization of natural vegetation in numerical models needs elaboration to take into account  
97 the reconfiguration and the complex structure of the plants (e.g. Boothroyd et al. 2015; Solari et al. 2016;  
98 Shields et al. 2017).

99 Additional research is needed on the transport, erosion and deposition rates in flows with natural  
100 vegetation (e.g. Vargas-Luna et al. 2015b) since shear-stress based estimates used under unvegetated  
101 conditions (e.g. Schuurman et al. 2013; Kasvi et al. 2015) do not necessarily apply to vegetated flows  
102 where turbulence is mainly controlled by the vegetative drag (e.g. Nepf 2012). The scarce flume studies  
103 that provide sufficient characterization of the investigated natural plants (e.g. Thornton et al. 1997;  
104 Ganthy et al. 2015) reveal that the effect of vegetation properties on sediment transport is dampened  
105 under conditions of limited sediment supply (Manners et al. 2015). Although settling velocity is the  
106 main sediment property controlling deposition (e.g. López and García 1998; Arboleda et al. 2010),  
107 vegetation and large woody debris govern local overbank deposition rates and patterns (e.g. Jeffries et  
108 al. 2003). Further, vegetative influence on the advective and diffusive supply of suspended sediment SS  
109 (e.g. Sharpe and James 1998; Zong and Nepf 2011) generates cross-sectional and reach-scale variability  
110 in deposition patterns (e.g. Middelkoop and Asselman 1998; Arboleda et al. 2010). Despite the rich  
111 body of literature on floodplain deposition, the investigation by Corenblit et al. (2009) in a gravel-bed  
112 river remains one of the few experimental studies examining how various measurable, physically-based  
113 properties of natural riparian plant stands explain annual net erosion and deposition rates.

114 The present paper intends to provide an overview on the characterization of natural riparian plants  
115 for flow and suspended sediment transport modeling. For this purpose, data published by the authors  
116 and others are revisited for further analyses. The specific objectives are 1) to improve the  
117 parameterization of foliated riparian vegetation by considering both the complex plant structures and  
118 their reconfiguration, and 2) to determine how the properties of natural floodplain plant stands influence  
119 the net erosion and deposition of suspended sediment under real field conditions. Section 2 describes  
120 recent developments in modeling vegetative drag and its effects on flow structure, focusing on  
121 approaches that can be readily used in practical applications, and Section 3 presents an environmental  
122 compound channel where the approaches are applied. Section 4.1 demonstrates the applicability of a  
123 recently developed drag force parameterization (Eq. 2) for natural woody vegetation while Section 4.2  
124 shows how the associated methodology can be used in hydraulic and morphological modeling. Sections

125 4.3–4.4 reveal how the cross-sectional vegetative blockage factor, distance from the sediment supply  
 126 point, and the flow velocity within the vegetation governed sediment transport at the field site while  
 127 Section 4.5 provides new knowledge on the management of sediment transport and water quality using  
 128 vegetated floodplains.

129

## 130 2 Modeling vegetative drag and its influence on flow structure

### 131 2.1 Parameterizing the drag of foliated riparian plants

132 Vegetation can be characterized in hydraulic and morphological models by considering the drag forces  
 133 ( $F$ ) exerted by the plants:

$$F = \frac{1}{2} \rho C_D A_C u_C^{2+\chi} \quad (1)$$

136

137 where  $\rho$  is the density of the fluid,  $C_D$  is the drag coefficient of the object, and  $A_C$  is the characteristic  
 138 reference area of the object.  $u_C$  is the characteristic approach velocity, commonly taken as the mean flow  
 139 velocity in the vegetated layer. The  $\chi$  exponent was introduced to the velocity term in Equation 1 to be  
 140 able to describe the non-quadratic relationship between the drag force and flow velocity resulting from  
 141 the flexibility-induced reconfiguration. In conventional modeling, plants are typically considered to be  
 142 rigid elements for which  $\chi=0$ , while natural woody vegetation exhibits values of  $\chi= -0.7 \dots -0.9$  in  
 143 foliated conditions and  $\chi= -0.2 \dots -0.5$  in leafless conditions at  $u_C \leq 1 \text{ m s}^{-1}$  (Jalonen and Järvelä 2014;  
 144 Västilä and Järvelä 2014; Whittaker et al. 2015).

145 Based on Eq. 1, several models taking into account the reconfiguration have been presented for  
 146 estimating the drag and flow resistance of woody vegetation. The models either use bulk  
 147 parameterizations that lump together the effects of the foliage and stem (e.g. Kouwen and Fathi-  
 148 Moghadam 2000; Järvelä 2004; Jalonen and Järvelä 2014; Whittaker et al. 2015) or have separate  
 149 parameterizations for these two differently behaving plant parts (Västilä and Järvelä 2014). In the model  
 150 of Västilä and Järvelä (2014), the characteristic reference areas are the total frontal projected area of the  
 151 woody trunk, branches and twigs ( $A_S$ ) for the stem and the total one-sided leaf area ( $A_L$ ) for the foliage.  
 152 The effect of the reconfiguration on the drag is taken into account with reconfiguration terms of the form  
 153  $(u_C/u_\chi)^\chi$ , where  $u_\chi$  is the reference velocity used for determining the reconfiguration parameter  $\chi$  (Västilä  
 154 and Järvelä 2014).  $u_\chi$  is recommended to be 0.05-0.2  $\text{m s}^{-1}$ , i.e. low enough to adequately capture the  
 155 reconfiguration while high enough to avoid uncertainty associated with the asymptotic nature of the  
 156 function close to 0  $\text{m s}^{-1}$ . The drag forces of reconfiguring woody plants can thus be expressed as

157

$$F = \frac{1}{2} \rho \left[ C_{D\chi,F} \left( \frac{u_C}{u_{\chi,F}} \right)^{\chi_F} A_L + C_{D\chi,S} \left( \frac{u_C}{u_{\chi,S}} \right)^{\chi_S} A_S \right] u_C^2 \quad (2)$$

158



159 where the subscripts  $F$  and  $S$  denote the parameters determined separately for the foliage and stem,  
 160 respectively. The drag coefficients  $C_{D\chi,F}$  and  $C_{D\chi,S}$  have a constant value despite reconfiguration (thus  
 161 the subscript  $\chi$ ), because the reconfiguration parameters  $\chi_F$  and  $\chi_S$  characterize the effect of the  
 162 reconfiguration on the drag at  $u_C$  in relation to the reference velocities  $u_{\chi,F}$  and  $u_{\chi,S}$ . Thus, the values of  
 163 all the six parameters should be documented (see e.g. Table 2 in Section 4.2). Eq. 2 is dimensionally  
 164 correct and it is applicable at  $u_C \approx 0.05\text{--}1.0 \text{ m s}^{-1}$  that are typical flow velocities on floodplains and river  
 165 banks. The physical factors affecting the parameter values are discussed in detail in Västilä and Järvelä  
 166 (2014).

167 We evaluated the performance of Equation 2 for predicting the drag forces of sapling-sized (0.9–3.1  
 168 m tall) woody plants (see Section 4.1). This validation included all the available literature data  
 169 containing the required leaf and stem areas. The data consist of towing tank measurements for nine  
 170 specimens of *Alnus glutinosa* (Common Alder; Xavier 2009; Dittrich et al. 2012; Jalonen and Järvelä  
 171 2014) and three specimens of *Betula pendula* (Silver Birch; Jalonen and Järvelä 2014), for which the  
 172 reference areas  $A_L$  and  $A_S$  had been determined. We used the values of  $\chi_F$ ,  $\chi_S$ ,  $u_{\chi,F}$ ,  $u_{\chi,S}$ ,  $C_{D\chi,F}$ , and  $C_{D\chi,S}$   
 173 derived by Västilä and Järvelä (2014) from independent data of the corresponding species (summarized  
 174 in Table 2 in Section 4.2).

175 Based on Eq. 2 and standard hydraulic theory (see Västilä 2015), we derived a physically solid pa-  
 176 rameterization for four coefficients or terms that are widely used in hydraulic and morphological mod-  
 177 eling and analyses ranging from one-dimensional (1D) considerations to depth-averaged 2D approaches  
 178 and 3D models (summarized in Table 1). For instance, 3D numerical models typically require represent-  
 179 ing the vegetation-induced source and sink terms, such as the momentum loss, as the vegetative drag  
 180 per unit volume (herein referred to as the drag–density parameter  $C_{Da}$ , where  $a$  is the vegetative refer-  
 181 ence area per unit volume). Based on Eq. 2,  $C_{Da}$  can be written for foliated woody vegetation as

$$182 \quad C_{Da} = C_{D\chi,F} \left( \frac{u_C}{u_{\chi,F}} \right)^{\chi_F} a_L + C_{D\chi,S} \left( \frac{u_C}{u_{\chi,S}} \right)^{\chi_S} a_S \quad (3)$$

183 where  $a_L$  and  $a_S$  equal  $A_L/(A_B z)$  and  $A_S/(A_B z)$  where  $z$  is the thickness of the examined layer. Further, the  
 184 drag–area parameter ( $C_{Da}H$ , where  $H$  is vegetation height, see e.g. Nepf 2012) that is used to  
 185 characterize the bulk vegetative drag in depth-averaged models is obtained by integrating Equation 3  
 186 over the inundated vegetation height:

$$187 \quad C_{Da}H = C_{D\chi,F} \left( \frac{u_C}{u_{\chi,F}} \right)^{\chi_F} \frac{A_L}{A_B} + C_{D\chi,S} \left( \frac{u_C}{u_{\chi,S}} \right)^{\chi_S} \frac{A_S}{A_B} \quad (4)$$

188  
 189 The vegetative Darcy–Weisbach friction factor ( $f''$ ) and Manning coefficient ( $n_{\text{veg}}$ ) are used to represent  
 190 stand- and reach-scale flow resistance and roughness in 1–2D models and computations:

191

$$f'' = 4 \left[ C_{D\chi,F} \left( \frac{u_C}{u_{\chi,F}} \right)^{\chi_F} \frac{A_L}{A_B} + C_{D\chi,S} \left( \frac{u_C}{u_{\chi,S}} \right)^{\chi_S} \frac{A_S}{A_B} \right] \quad (5)$$

193

$$n_{veg} = \frac{Kh^{1/6}}{\sqrt{2g}} \sqrt{C_{D\chi,F} \left( \frac{u_C}{u_{\chi,F}} \right)^{\chi_F} \frac{A_L}{A_B} + C_{D\chi,S} \left( \frac{u_C}{u_{\chi,S}} \right)^{\chi_S} \frac{A_S}{A_B}} \quad (6)$$

194

195

196 The usage of Eqs. 2–6 in flow and sediment transport modeling is discussed in detail in Section 4.2,  
 197 including the compiled parameter values for common riparian species (Table 2) and a description of the  
 198 work-flow (Fig. 7).

199

## 200 2.2 Hydraulic description of partly vegetated flows

201 Approaches for modeling flows where vegetation covers only part of the cross-section mostly have  
 202 complex descriptions for turbulence at the interfaces between vegetation and open water (e.g. Kang and  
 203 Choi 2006; Konings et al. 2012). By contrast, the two-layer model of Luhar and Nepf (2013) is  
 204 straightforward to apply as it describes the momentum balance using coefficients of drag at the  
 205 interfaces. This two-layer model was originally developed for patchy aquatic vegetation, but a simplified  
 206 version of the model was found to satisfactorily characterize the reach-scale flow resistance of a  
 207 vegetated compound channel (Västilä et al. 2016). The two-layer model describes the mean flow  
 208 velocities in the vegetated parts of the cross-section ( $u_v$ ) and in the open, unvegetated parts of the cross-  
 209 section ( $u_0$ ). The corresponding dimensionless flow velocities (equaling  $\sqrt{8/f}$  where  $f$  is the Darcy–  
 210 Weisbach friction factor) are denoted with an asterisk. To be applicable to compound geometry, the  
 211 model of Luhar and Nepf (2013) can be modified by replacing the channel width by the wetted perimeter  
 212 ( $P$ ) and the water depth by the hydraulic radius ( $R$ ) for the unvegetated and vegetated sections as:

213

$$u_0^* = \frac{u_0}{(gSR)^{1/2}} = \left[ \frac{2P(1-B_X)}{C_f L_b + C_v L_v} \right]^{1/2} \quad (7)$$

216

$$u_v^* = \frac{u_v}{(gSR)^{1/2}} = \left[ \frac{2PB_X + C_v L_v (u_0^*)^2}{C_D a PR B_X} \right]^{1/2} \quad (8)$$

220 where  $g$  is gravitational acceleration and  $S$  is energy slope.  $B_X$  is cross-sectional vegetative blockage  
 221 factor that is defined at different water levels as the wetted cross-sectional area covered by vegetation  
 222 ( $A_v$ ) divided by the total wetted cross-sectional area  $A_w$  (Fig. 1).  $C_f$  and  $C_v$  are drag coefficients  
 223 describing the bed shear stress and the shear stress at the interfaces between vegetation and open water,  
 224 respectively.  $L_b$  is the total length of the interface between the bed and open water, i.e., the total wetted

225 perimeter of the unvegetated part of the cross-section (Fig. 1).  $L_v$  is the total length of the interface  
226 between the vegetation and open water, i.e., the total wetted perimeter along the vegetation interface.  
227

### 228 2.3 Effects of vegetation on flow structure and transport processes

229 The effects of vegetation on the transport of suspended sediment can be evaluated through the  
230 advection–diffusion equation (e.g., López and García 1998; Sharpe and James 2006). However, it is not  
231 fully established how e.g. the diffusivities of suspended sediment or the erosion and deposition rates  
232 depend on the flexibility and density of the plant stands. Since turbulence and transport processes in  
233 vegetated flows are related to the vegetative drag (e.g. Nepf 2012), Luhar et al. (2008) describe the  
234 tendency of submerged vegetation to cause erosion or deposition by considering the effect of vegetation  
235 density on turbulence. Their framework is based on the analysis of the shear layer formed between  
236 vegetation and overflow, but a similar shear layer is typically observed at the interface between a  
237 vegetated floodplain and an unvegetated main channel (e.g., Kang and Choi 2006).

238 As summarized by Nepf (2012), for very sparse stands with the drag–area parameter  $C_{Da}H < 0.1$   
239 (where  $a$  is the frontal area of the plants per unit volume and  $H$  vegetation height), the vertical profile  
240 of the longitudinal mean flow velocity  $u_m(z)$  is logarithmic and turbulence is dominated by the vortices  
241 generated by the individual stems (pattern 1 in Fig. 2a). Increasing vegetation density results in the  
242 formation of an inflection point in the vertical velocity profile at the interface between vegetation and  
243 open water, so that turbulence within transitional ( $\sim 0.1 < C_{Da}H < \sim 0.23$ ) and dense ( $C_{Da}H > \sim 0.23$ ) plant  
244 stands is mainly generated by the shear-layer vortices (pattern 2 in Fig. 2b) that result from the velocity  
245 gradient (Nepf 2012). In sparse and transitional stands, turbulence levels are elevated near the bed, which  
246 is hypothesized to cause erosion or re-suspension of sediment (Luhar et al. 2008). In dense stands, the  
247 momentum transferred into the stand by the shear-layer vortices is dissipated by the high vegetative  
248 drag, and the low values of the flow velocity and near-bed turbulence may allow settling and deposition  
249 to take place (Fig. 2b).

250 The  $C_{Da}H$  limits (Fig. 2) of the approach are mainly based on data from stands of rigid cylinders and  
251 have not been validated for describing the effect of vegetation on net erosion or deposition. For natural  
252 flexible plant stands, the turbulent flow structure can be predicted e.g. with scaling relations (Sukhod-  
253 olov and Sukhodolova 2012) or second-order turbulence closures (Ayotte et al. 1999), but this requires  
254 reliable estimates of the drag–density parameter ( $C_{Da}$ , Eq. 3) at different mean flow velocities.  
255

## 256 3 Field investigation in a vegetated compound channel

### 257 3.1 Site and monitoring

258 A three-year field study was conducted at the Ritobäcken Brook (Sipoo, Finland), where a two-stage  
259 cross-section was formed by excavating a floodplain at the mean water level in winter 2010 (Fig. 3a).  
260 The two-stage approach was selected as an environmentally preferable alternative for improving the  
261 conveyance and thus the drainage of the surrounding agricultural fields. Details on the design and

262 construction are reported in Västilä and Järvelä (2011). The floodplain is 850 m long and 4–5 m wide  
263 while the main channel is ~2 m wide at bankful conditions. The longitudinal bed slope of the main  
264 channel is 0.001–0.002, and the cross-sectional mean velocities range at 0.1–0.3 m s<sup>-1</sup>. Agricultural  
265 fields comprise 13% of the 10 km<sup>2</sup> catchment area while the remainder is mainly forests and mires. The  
266 fields, channel bed and channel margins are mainly composed of clay and silt (Västilä and Järvelä 2011;  
267 Västilä et al. 2016).

268 Five 20 m long, differently vegetated sub-reaches were established within a 190 m long test reach in  
269 spring 2010 (Västilä and Järvelä 2011). The sub-reaches Grasses-D and -U were sown with pasture  
270 grasses, Grasses-N grew naturally established grasses, and Bare-M was intended to have bare soil.  
271 Willows-M grew Common Osier (*Salix viminalis*) planted at 0.5 m x 0.5 m spacing. Despite cutting the  
272 grassy floodplain and bank vegetation of Willows-M and Bare-M before the seasons when overbank  
273 flows occurred, sparse ≤0.05 m high stubble of grass remained in these sub-reaches. Both the low flow  
274 channel and the two-stage test reach are fairly straight (e.g. Fig. 4).

275 Site monitoring, with details reported in Västilä et al. (2016), included repeated cross-sectional sur-  
276 veys in two cross-sections of each sub-reach (Fig. 4) in three consecutive years to determine the annual  
277 net deposition. The cross-sectional geometry was measured at 0.2–0.4 m intervals in altogether 200  
278 points with a point gauge, and the accuracy in determining the ground level was ± 6 mm. The fluffy bed  
279 prevented obtaining reliable measurements of the vertical changes in the main channel. The water levels  
280 of the sub-reaches were recorded at different flows (Fig. 4). Vegetation height was determined for the  
281 sub-reaches every spring and autumn while vegetation dry mass and frontal area per unit volume were  
282 determined every autumn. To compute the transported loads of suspended sediment, sensors recorded  
283 water levels and turbidities at 5-minute intervals at continuous monitoring stations located at the up-  
284 stream and downstream ends of the 190 m long test reach (Fig. 4). Discharge and suspended sediment  
285 concentration were obtained from the sensor readings using site-specific rating curves (Västilä et al.  
286 2016).

287 Eight water samples were collected at different flow events with suspended sediment concentration  
288 of SSC=60–320 mg l<sup>-1</sup> from the downstream station (Fig. 4). During the sampling, floodplain water  
289 depth was ≤0.30 m and relative depth (floodplain water depth divided by the total water depth) ≤0.38.  
290 In the laboratory, the samples were subjected to laser-based analyses (LS 13 320 MW by Beckman  
291 Coulter) with a 5-min ultrasound pre-treatment. The dispersed suspended sediment had  $D_{10}=0.48 \mu\text{m}$   
292 (standard deviation SD=0.06),  $D_{50}=2.6 \mu\text{m}$  (SD=0.6), and  $D_{90}=11 \mu\text{m}$  (SD=2.5), with all the particles  
293 finer than 33  $\mu\text{m}$ . To give an indication on the cohesion that markedly affects the behavior of SS (e.g.  
294 Droppo 2001), suspended sediment was also analyzed in the flocculated form after only gentle mixing.  
295 Similar to Thonon et al. (2005), the average effective grain sizes were 2–4 times greater than in the  
296 dispersed form:  $D_{10}=1.3 \mu\text{m}$  (SD=0.6),  $D_{50}=7.8 \mu\text{m}$  (SD=1.1), and  $D_{90}=39 \mu\text{m}$  (SD=6), with no  
297 relationship to SSC. However, we acknowledge that these effective sizes determined in the laboratory  
298 may somewhat differ from the actual *in situ* values. Composite samples of the top 1 cm of the sediment

299 deposited on the middle of the floodplain were collected in the sub-reaches Grasses-U and Bare-M  
300 shortly after the monitoring ended. After drying at 105 °C and gentle crushing, the dispersed particle  
301 size distribution was analyzed using both the hydrometer method and the laser-based method with a 5-  
302 min ultrasound pre-treatment. The organic content was ~10% for the floodplain and bed sediment and  
303 15–43% for the suspended sediment.

304 Settling velocities ( $w_s$ ) were estimated for the SS flocs of different sizes using the relationship  
305 determined by Thonon et al. (2005) for cohesive suspended flocs of approximately similar size  
306 distribution:  $w_s=2.7\times 10^{-7}D^{1.57}$ , where  $D$  is the floc diameter in  $\mu\text{m}$  and  $w_s$  has the unit  $\text{m s}^{-1}$ . The length  
307 scales over which SS flocs of different sizes are advected before being deposited ( $x_a$ ) were computed as  
308  $x_a= u_v H/w_s$  (Zong and Nepf 2011) using the estimated  $w_s$ , the representative  $h=0.25$  m and the associated  
309  $u_v=0.027$   $\text{m s}^{-1}$  (mean value for the grassy sub-reaches obtained as described in Section 3.2). We obtained  
310 an estimate of the percentage of SS depletion within long, wide plant stands by dividing the distance to  
311 the SS replenishment point by the advection length scale.

312

### 313 3.2 Modeling and analyses

314 The differences in the vegetation properties and rates of deposition between the excavated bank, inner  
315 floodplain, and the ~1.2 m floodplain–main channel interface region are reported by Västilä et al. (2016)  
316 whereas the present paper focuses on the relevant physical processes at the reach scale. Thus, the data  
317 were spatially averaged at the cross-sectional or sub-reach scale for the present modeling and analyses,  
318 assuming Grasses-N to be representative of the areas located outside of the sub-reaches.

319 The flow velocities and discharges within floodplain vegetation as well as the total discharges on the  
320 floodplain were modelled using the approaches presented in Section 2. We firstly computed (Eqs. 7–8)  
321 the dimensionless velocities  $u_0^*$  and  $u_v^*$  using the values of  $L_b$ ,  $L_v$ ,  $P$ ,  $R$ ,  $B_x$  and  $a$  available from the  
322 cross-sectional and vegetation surveys. The velocities are representative of the summer/autumn condi-  
323 tions as  $a$  was analyzed in autumn when overbank flows with high SSC occur (Västilä and Järvelä 2011).  
324 We assumed  $C_f=C_v$ , as supported by Luhar and Nepf (2013), and used  $C_f=C_v=0.079$  according to the  
325 calibration of a simplified version of the model to the same site (Västilä et al. 2016). For the *S. viminalis*  
326 willows,  $C_{Da}$  was expressed according to Eq. 3, using the  $a_L$  and  $a_S$  determined through *in-situ* sampling  
327 and the  $\chi$  and  $C_{D\chi}$  values obtained for the same species in independent laboratory experiments (Västilä  
328 and Järvelä 2014; see Table 2 in Section 4.2). For the grassy vegetation, we determined  $a$  as the frontal  
329 projected area per unit volume of the grass blades through *in-situ* sampling and used the commonly  
330 assumed  $C_D=1$  and  $\chi=0$  (e.g. Luhar and Nepf 2013) as the grasses were observed to behave fairly rigidly  
331 at the low flow velocities ( $u_v=0.02$ – $0.06$   $\text{m s}^{-1}$  for the grassy vegetation, see Section 4.3). Sensitivity  
332 analyses were conducted for the grasses using  $C_D=0.5$  and  $C_D=1.5$ .

333 The discharges within the vegetation ( $Q_v$ ) and in the open part of the cross-section ( $Q_o$ ) were esti-  
334 mated by multiplying the measured bulk discharge ( $Q$ ) by the predicted shares of the discharge,  $Q_v =$

335  $Qu_v^*B_X / [u_v^*B_X + u_0^*(I - B_X)]$  and  $Q_0 = Qu_0^*(I - B_X) / [u_v^*B_X + u_0^*(I - B_X)]$ , respectively. The flow veloci-  
336 ties were derived as  $u_v = Q_v / (B_X A_w)$  instead of  $u_v = u_v^*(gSR)^{1/2}$  (Eq. 8), because the relative errors were  
337 expected to be lower for  $Q$  than for the  $(gSR)^{1/2}$  term. For emergent vegetation, the discharge on the  
338 floodplain ( $Q_{fp}$ ) equals  $Q_v$  while for submerged vegetation  $Q_{fp}$  was computed by summing  $Q_v$  and the  
339 discharge above the vegetation computed from  $u_0$ .

340 The significance of different factors for explaining the mean annual net erosion and deposition on  
341 the excavated floodplain and bank was evaluated with multiple regression analysis. Sediment properties  
342 were expected to be approximately constant because the sub-reaches were located close to each other  
343 (Fig. 4), with 94.5% of the incoming sediment load passing the entire reach without being deposited  
344 (see Fig. 11). Thus, the particle settling velocities and bulk sediment loads were assumed to be similar  
345 in all sub-reaches and were not directly included in the statistical analysis. Based on the observations of  
346 Västilä et al. (2016), the primary investigated factors were the cross-sectional vegetative blockage factor  
347 ( $B_X$ ), the distance from the nearest upstream suspended sediment replenishment point, and the flow ve-  
348 locity within floodplain vegetation ( $u_v$ ).

349 We used the mean values of  $B_X$  and  $u_v$  in the regression analysis as the continuous monitoring data  
350 showed that deposition occurred at all relative depths (floodplain water depth divided by the total water  
351 depth) after vegetation cover had been established.  $B_X$  was determined based on 14 overbank flow events  
352 for which data could be recorded during the two years, with floodplain water depth ranging at  $h=0-0.51$   
353 m (averaging 0.16 m), relative depth ranging at 0–0.51, and relative submergence (floodplain water  
354 depth divided by floodplain vegetation height) ranging at ~0–10.  $u_v$  was computed over all four recorded  
355 overbank flow events in autumn 2011 (autumn 2010 was so dry that no notable overbank flow events  
356 occurred), with floodplain water depth ranging at 0.07–0.51 m and averaging 0.30 m. The SS replenish-  
357 ment point is defined as a sub-reach allowing efficient supply of sediment to the floodplain via lateral  
358 advection from the main channel. For the observed mean floodplain water depth of 0.16 m, the computed  
359 discharge on the floodplain increased in the sparsely vegetated sub-reaches Bare-M and Willows-M (see  
360 Fig. 9), indicating the presence of diverging flows from the main channel in these sub-reaches. A less  
361 pronounced increase in discharge was obtained for the sub-reaches Grasses-D and -U at the highest  
362 water levels. Supported by visual observations, the sub-reaches Bare-M and Willows-M were consid-  
363 ered as SS replenishment points.

364 The multiple regression analysis was conducted with SPSS Statistics 23 with probability  $p < 0.05$   
365 considered as statistically significant. The residuals approximately fulfilled the assumption of homosce-  
366 dasticity. The residuals were not normally distributed as there were some outliers at both ends. For  
367 instance, fairly high net erosion (up to  $0.08 \text{ m a}^{-1}$ ) was recorded in several cross-sections at mid-bank  
368 level (see Fig. 3b) while fairly high net deposition (up to  $0.15 \text{ m a}^{-1}$ ) was measured lower on the bank  
369 or at the bank toe in the same cross-sections. These high values were expected to be caused by geotech-  
370 nical erosion while the morphological changes were mostly lower on the floodplain that was merely  
371 subjected to hydraulic processes.

372

## 373 4 Results and discussion

### 374 4.1 Performance of Equation 2 in predicting the drag forces of natural woody plants

375 Figure 5 shows the performance of Eq. 2 in predicting the drag forces of 0.9–3.1 m tall woody plants of  
376 two common species. The measured mean drag force at each examined mean flow velocity (Fig. 5a)  
377 was compared to the mean drag predicted by Eq. 2 with the values of  $\chi_F$ ,  $\chi_S$ ,  $u_{\chi,F}$ ,  $u_{\chi,S}$ ,  $C_{D\chi,F}$ , and  $C_{D\chi,S}$   
378 obtained from independent data by Västilä and Järvelä (2014) for the same two species (see Table 2).  
379 The mean relative errors were 26% and 14% for the foliated and leafless specimens, respectively (Fig.  
380 5b). The root mean square error and Nash–Sutcliffe efficiency were 1.18 and 0.85, respectively, for  
381 foliated specimens, and 0.74 and 0.88, respectively, for leafless specimens. The errors are higher at flow  
382 velocities exceeding the range of 0.05–1.0 m s<sup>-1</sup> recommended for the model (see Jalonen and Järvelä  
383 2014).

384 The measured data exhibited  $\chi_S = -0.2 \dots -0.47$  (as determined with Eq. 1) under leafless conditions  
385 and the bulk reconfiguration of  $\chi = -0.58 \dots -0.83$  under foliated conditions at  $u_m = 0.1–1.0$  m s<sup>-1</sup>. Thus,  
386 the plants showed notable reconfiguration particularly in the foliated condition, so that the rate of in-  
387 crease in drag with velocity (Fig. 5a) was notably lower compared to the squared rate of increase for  
388 rigid cylinders (for which  $\chi = 0$ ). The error in  $\chi_S$  predicted by the model was 0.07–0.15 for each leafless  
389 data series while the error in the predicted bulk  $\chi$  for each foliated data series was 0.02–0.03. Thus, the  
390 model (Eq. 2) captured the reconfiguration of the plants reliably, whereas the common assumption of  
391 plants being rigid cylinders fails to represent it.

392 Figure 5 together with the model validation for woody plants with heights of 0.2–0.7 m (Västilä and  
393 Järvelä 2014) demonstrate that the same values of the parameters  $\chi_F$ ,  $\chi_S$ ,  $u_{\chi,F}$ ,  $u_{\chi,S}$ ,  $C_{D\chi,F}$ , and  $C_{D\chi,S}$  were  
394 able to satisfactorily predict drag forces across a range of over three orders of magnitude (0.05–60 N),  
395 with the height of the specimens ranging over one order of magnitude. The apparent size-independency  
396 of the model parameters is mainly explained by the separate parameterization of both the foliage and  
397 stem, which accommodates the fact that the leaf-area-to-stem-area-ratio and thus the share of the foliage  
398 drag to the total drag notable decrease as tree height increases [see e.g. Västilä and Järvelä (2014) and  
399 Jalonen and Järvelä (2014) and references therein]. Further, the reconfiguration parameters of the foliage  
400 and stem seemed size-independent at the branch and sapling level (Jalonen and Järvelä 2014) although  
401 the flexural rigidities of the woody parts of trees generally increase with tree height and age (Niklas  
402 1997; Jalonen and Järvelä 2014).

403

### 404 4.2 Using the proposed parameterization in flow and sediment transport modeling

405 In this section we demonstrate how the proposed parameterization for woody vegetation (Eqs. 2–6,  
406 Figure 6) can be used in hydraulic and morphological models and analyses at plant, plant stand and  
407 reach scales. The proposed parameterization is applicable at different levels of relative submergence  
408 ( $h/H$ ) as long as a suitable approach velocity ( $u_c$ ) is selected (see Fig. 6). The  $C_{D\alpha}$  values can be fed into

409 3D models (e.g. Lopéz and García 1998; Kang and Choi 2006) or used in analytical models for emergent  
410 vegetation (e.g. Vargas-Luna et al. 2015b) while the  $C_{Da}H$  values can be applied when submerged plant  
411 stands are analyzed with so-called two-layer approaches (e.g. Luhar et al. 2008; Konings et al. 2012;  
412 Luhar and Nepf 2013; Vargas-Luna et al. 2015b). The  $f'$  or  $n_{veg}$  values can be used to represent  
413 vegetative roughness or vegetative component of the flow resistance in 1–2D models and computations  
414 (e.g. McGahey et al. 2008), including HEC-RAS.

415 With the separate description of the foliage and stem, the parameterization acknowledges the fact  
416 that woody plant parts and foliage behave differently under flow. Eqs. 2–6 can therefore be used at  
417 different foliation conditions, which allows e.g. estimating the seasonal differences in flow resistance  
418 that mainly result from leaf shedding. In addition, the parameterization can also support ecological  
419 studies on the effects of erosion and deposition on plant survival (e.g. Pasquale et al. 2014) or on  
420 ecosystem engineering by vegetation (e.g. Gurnell 2014). The proposed approach may also be useful  
421 for modeling wind flows within tree canopies (e.g. Ayotte et al. 1999; Peltola 2006; Belcher et al. 2012)  
422 although further analyses are required to confirm the proper scaling of the parameters for air flows.

423 Table 2 shows the values of the parameters  $\chi_F$ ,  $\chi_S$ ,  $u_{\chi,F}$ ,  $u_{\chi,S}$ ,  $C_{D\chi,F}$ , and  $C_{D\chi,S}$  for seven common species  
424 and four genera of riparian bushes and trees. The values were derived for *Alnus glutinosa*, *Betula*  
425 *pendula*, *Salix alba* × *Salix fragilis*, *Salix viminalis* (the same species that was planted at the present  
426 field site), and *Populus nigra* by Västilä and Järvelä (2014), and for *Betula pubescens* and *Salix caprea*  
427 by re-analyzing the data of Jalonen and Järvelä (2014). The values were determined by using the same  
428 reference velocities ( $u_{\chi,F}=u_{\chi,S}=0.2 \text{ m s}^{-1}$ ) and velocity range (up to  $u_m=0.8 \text{ m s}^{-1}$ ) for all species. The inter-  
429 specific variation in the parameter values (Table 2) is caused not only by measurement uncertainty and  
430 subtle differences in the hydrodynamic behavior between species, but also by slight differences in the  
431 research methodology between the two studies. For instance, the lower stem drag coefficients for the  
432 species examined by Jalonen and Järvelä (2014) are expected to be largely explained by the usage of the  
433 projected one-sided stem area as the reference area as opposed to the frontal projected stem area used  
434 by Västilä and Järvelä (2014).

435 Table 2 includes the species-averaged parameter values computed on the basis of the seven analyzed  
436 species. Depending on the species, using the species-averaged instead of the species-specific values  
437 causes a mean absolute error of 1–14% (mean: 8%, max: –17%) in the predictions for leafless vegetation  
438 and a mean absolute error of 3–30% (mean: 16%, max: 38%) for foliated vegetation assuming  $A_I/A_S=15$   
439 based on Jalonen and Järvelä (2014). The associated errors for foliated vegetation decrease as the share  
440 of the foliage drag to the total drag, or  $A_I/A_S$ , decreases because the relative inter-specific differences  
441 are greater in the foliage drag coefficient ( $C_{D\chi,F}$ ) than the stem drag coefficient ( $C_{D\chi,S}$ ). Overall, it appears  
442 feasible to use the species-averaged values in practical applications when riparian areas are populated  
443 by a mixture of species. We acknowledge that the parameter values may vary according to e.g. plant  
444 size, growth form, or season. Despite these uncertainties, the proposed parameterization provides more  
445 accurate and physically-based estimates of the drag of foliated vegetation compared to the commonly



446 made assumption of plants as rigid cylinders.

447 Figure 7 shows the work flow for estimating vegetative flow resistance using the proposed  
448 parameterization. In order to use Eqs. 2–6 for predictive purposes, the values of the parameters need to  
449 be known. Depending on the purpose and scale, the foliage and stem reference areas and densities are  
450 obtainable e.g. through spectral imaging (e.g. Zou et al. 2009), terrestrial laser scanning (e.g. Jalonen et  
451 al. 2015 and references therein; Ma et al. 2016), photographic methods or manual sampling, or literature  
452 data (e.g., Tables 2.5 and 3.8 in Zinke 2011; Table 2 in Jalonen et al. 2013). The parameters  $\chi_F$ ,  $\chi_S$ ,  $u_{\chi,F}$ ,  
453  $u_{\chi,S}$ ,  $C_{D\chi,F}$ , and  $C_{D\chi,S}$  representative of a given species can be derived from literature (e.g. Table 2) or  
454 from experimental data. Using the values from Table 2, the only additional vegetative properties needed  
455 for modeling are the foliage and stem reference areas or densities. The values of the vegetative flow  
456 resistance (Eqs. 2–6) need to be solved iteratively since the resistance and velocity are interconnected  
457 because of reconfiguration. Finally, resistance values computed through Eqs. 2–6 can be used as direct  
458 input to hydraulic and morphological computations and models, replacing the less representative but  
459 conventionally applied parameterization of plants as rigid cylindrical elements.

460 Deriving the values of  $\chi_F$ ,  $\chi_S$ ,  $u_{\chi,F}$ ,  $u_{\chi,S}$ ,  $C_{D\chi,F}$ , and  $C_{D\chi,S}$  experimentally requires either ( $f'$ ,  $u_C$ ) data of  
461 emergent or just submerged plant stands, or ( $\bar{F}$ ,  $u_C$ ) data, where  $\bar{F}$  denotes the average drag force over  
462 several specimens. These data should be obtained at both leafless and foliated conditions at a few  
463 relevant values of  $u_C$  covering a broad enough velocity range (e.g.  $u_C = 0.2\text{--}0.8\text{ m s}^{-1}$ ), with velocities of  
464 the order of  $0.05\text{--}0.2\text{ m s}^{-1}$  used as  $u_{\chi,F}$  and  $u_{\chi,S}$ . To ensure accuracy across the whole velocity range it is  
465 recommended that  $\bar{F}$  data are converted into  $f'$  values through  $f'' = 8\bar{F} / \rho u_C^2 A_B$  using the unit bed  
466 area ( $A_B = 1\text{ m}^2$ ). After determining the associated foliage and stem reference areas, the values of the  
467 parameters  $\chi_S$  and  $C_{D\chi,S}$  are obtained by fitting Eq. 2 to the ( $f'$ ,  $u_C$ ) dataset of the leafless specimens. The  
468 parameters  $\chi_F$  and  $C_{D\chi,F}$  are then derived by fitting Eq. 2 to the ( $f'$ ,  $u_C$ ) dataset of the foliated specimens  
469 and using the known values of  $\chi_S$  and  $C_{D\chi,S}$ . As the parameterization explicitly takes into account the  
470 reconfiguration through the terms  $(u_C/u_{\chi})^X$ , the drag coefficients and reconfiguration parameters remain  
471 constant at the considered velocity range.

472

### 473 4.3 Flow hydraulics and net deposition in the vegetated compound channel

474 Figure 8 shows the mean velocities within ( $u_v$ ) and above ( $u_0$ ) the floodplain vegetation modelled using  
475 the two-layer approach (Eqs. 7–8) with  $C_{Da}$  parameterized according to Eq. 3 for the willows. For the  
476 modelled flow events, the velocities were notably lower within dense high grasses ( $u_v=0.02\text{--}0.06\text{ m s}^{-1}$ ,  
477 averaging  $0.036\text{ m s}^{-1}$  for sub-reaches Grasses-N, -D, and -U with  $C_{Da}=7\text{--}24$  in autumn 2011) compared  
478 to sparser low grasses (mean  $u_v=0.072\text{ m s}^{-1}$  for Bare-M with  $C_{Da}=9$ ) and sparse willows (mean  $u_v=0.17$   
479  $\text{m s}^{-1}$  for Willows-M with  $C_{Da}=0.06\text{--}0.07$  above the layer of low grasses). According to the sensitivity  
480 analyses, the change of  $C_D=1$  by  $\pm 0.5$  altered the mean velocities of the grassy sub-reaches by up to few  
481  $\text{cm s}^{-1}$ :  $C_D=1.5$  resulted in  $u_v=0.02\text{--}0.06\text{ m s}^{-1}$  and  $C_D=0.5$  in  $u_v=0.03\text{--}0.08\text{ m s}^{-1}$ . The modelled discharge  
482 on the floodplain increased with increasing floodplain water depth, with the rate of increase notably

483 accelerating after the vegetation became submerged (Figure 9). Thus, the total discharge on the flood-  
484 plain at the highest water levels was lower for the emergent grassy vegetation (Grasses-N) compared to  
485 the submerged vegetation (Grasses-D and -U) for which water flowed mainly above the top of the veg-  
486 etation with high flow velocities in the unvegetated parts of the cross-section (Fig. 8).

487 Figure 10 shows the measured mean annual net deposition across the floodplain and bank as derived  
488 from the cross-sectional surveys. The factors explaining net deposition are compiled into Table 3. The  
489 multiple regression analysis revealed that the net deposition was significantly correlated with the mean  
490 cross-sectional vegetative blockage factor ( $B_x$ ,  $p < 0.001$ ), distance from the suspended sediment replen-  
491 ishment point ( $x_s$ ,  $p = 0.009$ ), and the estimated mean flow velocity within the vegetation ( $u_v$ ,  $p = 0.006$ ).  
492 The regression explained most of the variation in the observed mean net deposition in the ten cross-  
493 sections (adjusted  $r^2 = 0.57$ , Fig. 10), indicating that  $u_v$ ,  $B_x$ , and  $x_s$  were the main factors describing the  
494 vegetation-induced differences in bulk erosion and deposition. The physical processes captured in the  
495 three investigated factors are expected to qualitatively explain the bulk influence of vegetation on net  
496 deposition at other sites, as well, (see Section 4.4) although detailed predictions of spatial deposition  
497 patterns require considering the turbulent flow structure. Net deposition is also affected by sediment  
498 properties, with higher particle settling velocities and incoming sediment loads increasing the rate of  
499 deposition (Table 3; e.g. Arboleda et al. 2010).

500 The particle size distribution of the dispersed, deposited sediment varied depending on the analysis  
501 method (Figure 11). Both the hydrometer and laser-based methods resulted in roughly similar share of  
502 coarse silt and sand (82 vs 74% finer than 45  $\mu\text{m}$  for Grasses-U and 70 vs 76% finer than 47  $\mu\text{m}$  for  
503 Bare-M) but different share of clay (39 vs 11% finer than 2  $\mu\text{m}$  for Grasses-U and 34 vs 12% for Bare-  
504 M). The share of the clay fraction is known to be under-estimated by the laser-based method and over-  
505 estimated by the settling-based hydrometer method (e.g. Di Stefano et al. 2010). Averaging the results  
506 of the two methods, the  $D_{50}$  and  $D_{70}$  values were 18–32% lower for the dense, high grassy vegetation in  
507 Grasses-U ( $D_{50} = 7.4 \mu\text{m}$  and  $D_{70} = 27$ ) compared to the sparsely vegetated Bare-M ( $D_{50} = 9.1 \mu\text{m}$  and  
508  $D_{70} = 39$ ).

509 The computed advection length scales were 16600 m, 990 m and 79 m for the effective floc sizes of  
510 1.3  $\mu\text{m}$ , 7.8  $\mu\text{m}$  and 39  $\mu\text{m}$  ( $D_{10}$ ,  $D_{50}$  and  $D_{90}$  of the SS), respectively, with the corresponding settling  
511 velocities of 0.15  $\text{cm h}^{-1}$ , 2.4  $\text{cm h}^{-1}$ , and 31  $\text{cm h}^{-1}$ . As an example, the computations showed that 19%,  
512 49% and 92% of the 39  $\mu\text{m}$  flocs were deposited before the flow entered the measured cross-sections in  
513 the Grasses-U, -N and -D with the mean distances of 15 m, 39 m and 73 m, respectively, to the SS  
514 replenishment point. 5%, 12% and 20% of the total SS load on the floodplain was estimated to be de-  
515 posited before the flow entered the three sub-reaches. The settling velocities estimated with the relation-  
516 ship of Thonon et al. (2005) for the effective flocculated  $D_{10}$ – $D_{90}$  were 1.4–3.5 times higher than those  
517 estimated with the Stokes equations for the dispersed  $D_{10}$ – $D_{90}$ . The estimated percentages of sediment  
518 deposited are directly related to the settling velocity, which highlights the importance of properly con-  
519 sidering the flocculation.

520

#### 521 4.4 Physical reasoning of the factors explaining the influence of vegetation on net deposition

522 The present investigation is one of the few studies that experimentally determined how measurable,  
523 hydraulically solid properties of natural plant stands control erosion and deposition rates of suspended  
524 sediment under real field conditions. The present channel has a low bed slope (0.001) and the estimated  
525 flow velocities were fairly low within all floodplain plant stands (Figure 8), and thus the site can be  
526 generally classified as a depositional environment. The stream power ( $\Omega$ ) of the 190 m long test reach  
527 (based on median annual maximum discharge as estimated from a region-specific empirical nomogram)  
528 is approximately  $16 \text{ W m}^{-1}$ , falling close to the regime characterized by long-term storage of fines within  
529 vegetation ( $\Omega < 10 \text{ W}^{-1}$ ) as observed in UK rivers by O'Hare (2015).

530 Net deposition increased with decreasing mean flow velocity within vegetation (Table 3). Thus, the  
531 high vegetation densities ( $C_{Da}$ ) causing low flow velocities (Figure 8) prevented sediment from being  
532 eroded or re-suspended from the floodplain and promoted deposition. The modelled velocities within  
533 the vegetation and in the unvegetated part of the cross-section indicated that a vertical shear layer was  
534 formed at the top of vegetation when water depth exceeded vegetation height, and another shear layer  
535 was formed between the unvegetated main channel and the vegetated floodplain. Although the two-layer  
536 model cannot resolve the detailed flow structure in the shear layer, Figure 8 shows that the velocity  
537 gradient was stronger for denser vegetation (Grasses-U, -D) compared to sparser, lower vegetation  
538 (Bare-M). As schematized in Fig. 2b, the shear layer vortices cannot penetrate to the bottom at high  
539 vegetation densities (Nepf 2012), which results in low near-bed turbulence within submerged stands.

540 The spatially-averaged data revealed that net erosion occurred in the sub-reach Bare-M where the  
541 two-year mean spatially-averaged values were  $\sim 0.02 \text{ m}$  for the vegetation height ( $H$ ) and  $0.19$  for the  
542 drag-area parameter ( $C_{Da}H$ ). By contrast, net deposition occurred in the remaining four sub-reaches  
543 with two-year mean  $C_{Da}H = 0.38\text{--}4.9$  and  $H = 0.14\text{--}0.77 \text{ m}$ . These figures were in agreement with the  
544 literature value of  $C_{Da}H \approx 0.23$  as a density limit between erosion and deposition of suspended sediment  
545 (see Fig. 2; Luhar and Nepf (2008)), which supports the applicability of the framework for preliminary  
546 estimation of the fate of SS under natural vegetative conditions. In the future, more detailed analyses on  
547 the flow structure are needed in particular to determine the lateral transfer of momentum and SS between  
548 flexible vegetation and adjacent open water.

549 Net deposition increased with increasing cross-sectional vegetative blockage factor ( $B_x$ , Table 3).  
550 The examined compound channel had fairly homogeneous cross-sections, and therefore the vegetative  
551 blockage factor was directly related to the height of the floodplain vegetation. In the study of Corenblit  
552 et al. (2009) in a gravel-bed river, two-year net erosion and deposition within riparian stands were sig-  
553 nificantly correlated only with the intercepted biovolume that essentially corresponds to the maximum  
554 inundated height for a relatively homogeneous plant cover as in the present case. Thus, the present study  
555 strengthens the evidence on the importance of vegetation height, or vegetative blockage at cross-sec-  
556 tional level considerations, in controlling the net deposition within vegetated flows (see also Ganthy et

557 al. 2015). The modeling showed that the discharge passing through vegetation increased with increasing  
558 water level until vegetation became submerged (see Fig. 9 where  $Q_{fp}=Q_v$  under emergent conditions)  
559 and remained fairly constant for higher water levels. Thus, increasing vegetative height (and blockage)  
560 enhances the availability of sediment for deposition by increasing the advective supply of SS to the  
561 vegetated area (see also Peralta et al. 2008). While the study of Corenblit et al. (2009) considered vege-  
562 tative parameters corresponding to annual maximum flows, our results indicated that the usage of the  
563 annual mean blockage factor was justified for conditions where notable deposition occurred at flow  
564 events of different magnitudes.

565 Net deposition decreased as the distance from the point where sediment is laterally advected onto the  
566 floodplain increased ( $x_s$ , Table 3), confirming the importance of the longitudinal advective SS supply in  
567 controlling the deposition rate. Because of deposition, the availability of SS within vegetation markedly  
568 decreases away from the main sediment source since diffusion can supply SS across a limited distance  
569 only (e.g. Arboleda et al. 2010; Zong and Nepf 2011). The significant correlation between  $x_s$  and net  
570 deposition indicated that the lateral diffusion from the main channel and the vertical diffusion from the  
571 overflow through shear-layer vortices (see Fig. 2b) could not compensate for the deposition-induced  
572 decrease in the sediment load on the inner floodplain. The supply of SS through lateral diffusion was  
573 limited mainly to the 1.2 m wide main channel–floodplain interface: for the two sub-reaches located  
574 farther away from the SS replenishment point, deposition on the inner floodplain was less than half (on  
575 average  $0.5 \text{ cm a}^{-1}$ ) of that on the interface ( $1.3 \text{ cm a}^{-1}$ ) despite vegetation height and density differing  
576 by less than 20%. The advection length scales indicated that larger flocs rapidly became depleted as  
577 water flowed on the floodplain, resulting in finer deposits after a distance of 15 m from the point where  
578 the lateral flow of SS from the main channel entered the floodplain (Figure 11). The estimates on the  
579 depletion of SS along the floodplain (Section 4.3) were expected to be roughly representative of other  
580 small lowland floodplains with similar flow velocities.

581 Overall, our study showed that net deposition of fines within riparian vegetation is determined by the  
582 interplay between sediment supply, effective particle size distribution and the associated settling veloc-  
583 ities, and the flow velocity within the vegetation (Table 3). Although deposition has been found to be  
584 primarily governed by plant density in small-scale flume studies (Thornton et al. 1997) and in intertidal  
585 environments with plant patches (e.g. Bos et al. 2007), not even dense riparian vegetation generates  
586 much deposition if there are supply-limited conditions caused by continuous plant stands. On the other  
587 hand, if large sediment flocs are supplied, even stands of a relatively low vegetation density (e.g. the  
588 present willows with  $C_D aH=0.38$ ) can promote notable deposition at environments characterized as dep-  
589 ositional based on e.g. stream power. The effect of vegetation properties on net deposition is expected  
590 to remain qualitatively similar for larger rivers as for the present 10 m wide channel (Table 3). However,  
591 quantitative differences are expected because wider floodplains limit the lateral sediment supply more  
592 strongly (e.g. Arboleda et al. 2010). In addition, the water depths are higher and the relative submergence  
593 of vegetation may be lower for grassed floodplains of larger rivers, which can lead to more efficient

594 vertical supply of SS to the plant stands.

595

#### 596 4.5 Implications for sediment management and water quality

597 Sections 4.3–4.4 show evidence that floodplains inundated at medium to high flows allow managing the  
598 transport of fine suspended sediment through suitable maintenance of floodplain vegetation. For in-  
599 stance, vegetative dry mass and height above approximately  $200 \text{ g m}^{-2}$  and  $0.1 \text{ m}$ , respectively, were the  
600 thresholds for cohesive sediment deposition within natural grasses (Fig. 10; see also Figure 7 in Västilä  
601 et al. 2016). Further, the recorded near-bed values of the vegetation density ( $a$ ) together with the ap-  
602 proach of Luhar et al. (2008) summarized in Fig. 2 allow estimating the height of natural grassy vege-  
603 tation required to prevent erosion. The near-bed  $a$  ranged at 6–26 in the five sub-reaches, indicating that  
604 a 4 cm high cover of natural grasses would function as erosion protection by exceeding the density limit  
605 of  $C_D a H > 0.23$  proposed by Luhar et al. (2008). If the flow velocity is high enough to notably bend the  
606 grasses so that the drag coefficient decreases to  $C_D = 0.5$  in agreement with the sensitivity analysis, a  $\sim 10$   
607 cm high vegetation cover would be required.

608 We found that deposition can be supply-limited even on narrow (5 m wide in the present case) veg-  
609 etated floodplains with estimated settling velocities of as low as  $w_s \leq 31 \text{ cm h}^{-1}$  for the effective  $D_{10} - D_{90}$ .  
610 Further, the results suggested that low levees (longitudinal sediment deposits at the main channel-flood-  
611 plain interface) can be generated at sites where the suspended sediment is predominantly much finer  
612 than typically considered ( $w_s \geq 36 \text{ cm h}^{-1}$  in e.g. Sharpe and James 2006; Arboleda et al. 2010; Branß et  
613 al. 2016). The formation of levees can have significant implications on the water levels, lateral connec-  
614 tivity and the supply of substances on shallow floodplains. The generation of levees is strengthened by  
615 the presence of vegetation (Arboleda et al. 2010) but is also affected by the floodplain water depths: a  
616 sub-reach with the maximum relative depth of 0.38 led to  $\sim 5 \text{ mm/a}$  higher interfacial deposition than  
617 that with a maximum relative depth of 0.30 when the effect of vegetation was excluded statistically (see  
618 also discussion of Fig. 7 of Västilä et al. 2016). Such differences in the relative depth have been found  
619 important in the flume study of Branß et al. (2016), who report that levee width was halved when the  
620 relative depth decreased from 0.35 to 0.30.

621 The low flow channel of the test reach was fairly straight (see Fig. 4), and lateral advection of SS  
622 from the main channel took place only at floodplain areas with very low or sparse vegetation. A  
623 meandering two-stage channel planform could possibly enhance the supply of SS to the floodplains  
624 through flows crossing over from the main channel at bends although dense vegetation may reduce the  
625 efficiency of mixing compared to that observed for bare conditions (e.g. Shiono and Muto 1998). Under  
626 conditions of inefficient cross-sectional mixing, deposition can be enhanced by ensuring the supply of  
627 sediment e.g. through mowing floodplain vegetation from short, regularly-spaced sub-reaches along the  
628 channel while maintaining high plant stands elsewhere. By contrast, the supply of sediment, and  
629 consequently the deposition on the floodplain, can be reduced by maintaining continuous vegetation  
630 strips at the floodplain-main channel interface.

631 Figure 12 shows the suspended sediment mass balance in the compound test reach. The transported  
632 sediment load originated mainly from the catchment, with the fields estimated to have an approximately  
633 six times higher specific load than the forested areas (Västilä and Järvelä 2011). Annually, 5.5% of the  
634 incoming suspended sediment was deposited on the 190 m long floodplain with the spatially and  
635 seasonally averaged vegetation height of 0.25 m (Västilä et al. 2016). 89% of the total suspended  
636 sediment load of  $\sim 110 \text{ t a}^{-1}$  was transported at overbank flows, indicating that the floodplain at the mean  
637 water level appeared suitable for enhancing the water quality by trapping sediment. The entire  
638 compound reach was fairly homogeneous in vegetation, cross-sectional geometry, sediment load and  
639 sediment properties, and therefore we estimated a total annual SS trapping of  $\sim 20\%$  on the 850 m long  
640 floodplain based on direct up-scaling from the test reach.

641 The field study demonstrated that constructed floodplains offer potential for controlled deposition  
642 and water quality improvements as notable amounts of clay–medium silt are deposited facilitated by the  
643 flocculation of the cohesive primary particles (see Figure 11; Middelkoop and Asselman 1998; Thonon  
644 et al. 2005; Arboleda et al. 2010). Deposition of the cohesive fraction may reduce the loads of particle-  
645 bound phosphorus, pesticides, and heavy metals transported to downstream water bodies. For instance,  
646 most of the transported phosphorus is typically sorbed onto fine particles in catchments dominated with  
647 cohesive soils (e.g. Uusitalo et al. 2000; Västilä et al. 2015). On the other hand, the accumulation of  
648 contaminated sediment on floodplains may affect local ecology and the use of the floodplains for agri-  
649 culture, or the substances may be released back to the liquid phase through changes in water or soil  
650 chemistry. Deposition and vegetation development on excavated floodplains may decrease the convey-  
651 ance capacity of the channel over time (e.g., Geerling et al. 2008; Villada Arroyave and Crosato 2010),  
652 which necessitates vegetation management and periodic lowering of the floodplains. Despite these  
653 maintenance requirements, constructed floodplains are an environmentally viable alternative to conven-  
654 tional trapezoidal channels that require frequent, ecologically disturbing dredging of the channel bed  
655 (e.g. USDA 2007).

656

## 657 5 Conclusions

658 Sediment properties are known to be critical for reliable modeling of sediment transport, but the influ-  
659 ence of natural vegetation remains less researched. From this starting point we investigated the charac-  
660 terization of natural riparian vegetation for hydraulic and sediment transport analyses by using and  
661 amending recently proposed approaches. We combined detailed investigations at the laboratory and field  
662 scales, while seeking straightforward practical applicability using physically solid parameterizations. For  
663 instance, the field investigations showed that the cross-sectional vegetative blockage factor ( $B_x$ ) was  
664 statistically highly significant in determining the deposition rate for differently vegetated floodplain  
665 reaches. In parallel, a parameterization of vegetative drag force (Eq. 2) that incorporates the flexibility-  
666 induced reconfiguration was successfully validated for natural woody plants under laboratory condi-  
667 tions. Subsequently, we derived a physically-based parameterization (Eqs. 2–6) for five coefficients and

668 terms that are widely used in hydraulic and morphological modeling to represent the influence of vege-  
669 tation on flow resistance and structure (summarized in Table 1). The presented parameterization pro-  
670 vides a more realistic description of natural vegetation compared to the conventional rigid cylinder ap-  
671 proach, allowing reliable estimates under both leafless and foliated conditions. The proposed  
672 methodology (Fig. 7) is easy to apply: Eqs. 2–6 (Fig. 6) can be readily implemented into 1D–3D ana-  
673 lytical and numerical models using the values of the parameters compiled for common riparian trees and  
674 bushes (Table 2). Consequently, the usage of the presented approaches was successfully demonstrated  
675 for field-scale analyses.

676 The field site with cohesive soils and sediment provided new insight into the factors governing net  
677 deposition and erosion of fine sediment within natural riparian vegetation. The identified factors (the  
678 drag–area parameter  $C_{Da}H$  and the associated flow velocity within vegetation, the cross-sectional veg-  
679 etative blockage, and the distance from the sediment replenishment point) were shown to capture key  
680 processes and were thus expected to apply more broadly to explain the bulk influence of vegetation on  
681 deposition. The analyses implied that longitudinal advection was the most important mechanism sup-  
682 plying fine sediment to the floodplain plant stands although continuous stands can limit deposition.  
683 From a practical point of view, this study provided guidance on the management of fine sediment by  
684 discussing how riparian vegetation can be maintained in order to control erosion and deposition in en-  
685 vironmental channel designs. We believe that active vegetation maintenance offers further possibilities,  
686 and future studies should be directed towards determining the potential in controlling the fate of pollu-  
687 tants in water courses.

688

## 689 **References**

- 690 Aberle J, Järvelä J (2013) Flow resistance of emergent rigid and flexible vegetation. *J Hydraul Res*  
691 51(1):33–45. doi:10.1080/00221686.2012.754795
- 692 Aberle J, Järvelä J (2015) Hydrodynamics of vegetated channels. In Rowinski P, Radecki-Pawlik A  
693 (eds) *Rivers – physical, fluvial and environmental processes*. GeoPlanet: Earth and Planetary  
694 Sciences. Springer, Berlin, pp 519–541. doi:10.1007/978-3-319-17719-9\_21
- 695 Arboleda AM, Crosato A, Middelkoop H (2010) Reconstructing the early 19th century Waal River by  
696 means of a 2D physics-based numerical model. *Hydrol Process* 24(25): 3661–3675. doi:  
697 10.1002/hyp.7804
- 698 Ayotte KW, Finnigan, JJ, Raupach MR (1999) A second-order closure for neutrally stratified vegetative  
699 canopy flows. *Bound-lay. Meteorol* 90:189–216
- 700 Belcher SE, Harman IN, Finnigan JJ (2012) The wind in the willows: flows in forest canopies in  
701 complex terrain. *Annu. Rev. Fluid Mech* 44:479–504. doi: 10.1146/annurev-fluid-120710-101036
- 702 Bos AR, Bouma TJ, de Kort GLJ, van Katwijk MM (2007) Ecosystem engineering by annual intertidal  
703 seagrass beds: Sediment accretion and modification. *Estuar Coast Shelf S* 74:344–348.  
704 doi:10.1016/j.ecss.2007.04.006

705 Boothroyd RJ, Hardy RJ, Warburton J, Marjoribanks TI (2015) The importance of accurately  
706 representing submerged vegetation morphology in the numerical prediction of complex river flow.  
707 Earth Surf Process Landforms 41(4): 567–576. doi:10.1002/esp.3871

708 Branß T, Dittrich A, Núñez-González F (2016) Reproducing natural levee formation in an experimental  
709 flume. In Constantinescu G, Garcia M, Hanes D (eds) River Flow 2016. CRC Press, London, pp  
710 1122–1128

711 Corenblit D, Steiger J, Gurnell AM, Tabacchi E, Roques L (2009) Control of sediment dynamics by  
712 vegetation as a key function driving biogeomorphic succession within fluvial corridors. Earth Surf  
713 Process Landforms 34(13):1790–1810. doi:10.1002/esp.1876

714 de Langre E (2008) Effects of wind on plants. Annu Rev Fluid Mech 40:141–168

715 de Langre E, Gutierrez A, Cossé J (2012) On the scaling of drag reduction by reconfiguration in plants.  
716 C. R. Mecanique 340: 35–40. doi:10.1016/j.crme.2011.11.005

717 Di Stefano C, Ferro V, Mirabile S (2010) Comparison between grain-size analyses using laser diffraction  
718 and sedimentation methods. Biosystems Eng 106: 105–115.  
719 doi:10.1016/j.biosystemseng.2010.03.013

720 Dittrich A, Aberle J, Schoneboom T (2012) Drag forces and flow resistance of flexible riparian  
721 vegetation. In Rodi W, Uhlmann M (eds) Environmental Fluid Mechanics: Memorial Volume in  
722 honour of Prof. Gerhard H. Jirka, IAHR Monographs. CRC Press, London, pp 195–215

723 Droppo I (2001) Rethinking what constitutes suspended sediment. Hydrol Process 15:1551–1564.  
724 doi:10.1002/hyp.228

725 Fleischer P, Soyeaux R (2013) Technical-biological bank protection on waterways with high traffic  
726 frequency – first experience gained from a test stretch at the River Rhine with regard to bank stability.  
727 In Rigo P, Wolters M (eds.) Proceedings, 6<sup>th</sup> International PIANC-Smart Rivers Conference, 23–27  
728 September 2013, Liège, Belgium/Maastricht, the Netherlands. 10 pp

729 Ganthly F, Soissons L, Sauria PG, Verney R, Sottolichio A (2015) Effects of short flexible seagrass  
730 *Zostera noltei* on flow, erosion and deposition processes determined using flume experiments.  
731 Sedimentology 62:997–1023

732 Geerling GW, Kater E, van den Brink C, Baptist MJ, Ragas AMJ, Smits AJM (2008) Nature  
733 rehabilitation by floodplain excavation: The hydraulic effect of 16 years of sedimentation and  
734 vegetation succession along the Waal River, NL. Geomorphology 99(1–4):317–328

735 Gurnell A (2014) Plants as river system engineers. Earth Surf Process Landforms 39:4–25.  
736 doi:10.1002/esp.3397

737 Jalonen J, Järvelä, J (2014) Estimation of drag forces caused by natural woody vegetation of different  
738 scales. J Hydrodyn 26:608–623. doi:10.1016/S1001-6058(14)60068-8

739 Jalonen J, Järvelä J, Aberle J (2013) Leaf area index as vegetation density measure for hydraulic  
740 analyses. J Hydraul Eng 139(5):461–469. doi:10.1061/(ASCE)HY.1943-7900.0000700



741 Jalonen J, Järvelä J, Virtanen J-P, Vaaja M, Kurkela M, Hyyppä H (2015) Determining characteristic  
742 vegetation areas by terrestrial laser scanning for floodplain flow modeling. *Water* 7(2):420-437. doi:  
743 10.3390/w7020420

744 Järvelä J (2004) Determination of flow resistance caused by non-submerged woody vegetation. *Int J*  
745 *River Basin Manag* 2(1):61–70

746 Jeffries R, Darby SE, Sear DA, 2003. The influence of vegetation and organic debris on flood plain  
747 sediment dynamics: case study of a loworder stream in the New Forest, England. *Geomorphology*  
748 51, 61-80.

749 Kang H, Choi S-U (2006) Turbulence modeling of compound open-channel flows with and without  
750 vegetation on the floodplain using the Reynolds stress model. *Adv Water Res* 29:1650–1664

751 Kasvi E, Alho P, Lotsari E, Wang Y, Kukko A, Hyyppä H, Hyyppä J (2015) Two-dimensional and  
752 three-dimensional computational models in hydrodynamic and morphodynamic reconstructions of a  
753 river bend: sensitivity and functionality. *Hydrol Process* 29:1604–1629. doi: 10.1002/hyp.10277

754 Konings AG, Katul GG, Thompson SE (2012) A phenomenological model for the flow resistance over  
755 submerged vegetation. *Water Resour Res* 48, W02522. doi:10.1029/2011WR011000

756 Kouwen N, Fathi-Moghadam M (2000) Friction factors for coniferous trees along rivers. *J Hydraul Eng*  
757 126:732–740

758 Li M-H, Eddleman KE (2002) Biotechnical engineering as an alternative to traditional engineering  
759 methods: A biotechnical streambank stabilization design approach. *Landscape Urban Plan* 60:225–  
760 242

761 Li X, Zhang L, Zhang Z (2006) Soil bioengineering and the ecological restoration of riverbanks at the  
762 Airport Town, Shanghai, China. *Ecol Eng* 26:304–314. doi:10.1016/j.ecoleng.2005.10.011

763 López F, García M (1998) Open-channel flow through simulated vegetation: Suspended sediment  
764 transport modeling. *Water Resour Res* 34(9):2341–2352

765 Luhar M, Nepf H (2013) From the blade scale to the reach scale: A characterization of aquatic vegetative  
766 drag. *Adv Water Resour* 51:305–316. doi:10.1016/j.advwatres.2012.02.002

767 Luhar M, Rominger J, Nepf, H (2008) Interaction between flow, transport and vegetation spatial  
768 structure. *Environ. Fluid Mech.* 8:423–439

769 Ma L, Zheng G, Eitel JUH, Magney TS, Moskal LM (2016) Determining woody-to-total area ratio using  
770 terrestrial laser scanning (TLS). *Agr Forest Meteorol* 228–229:217–228. doi:  
771 10.1016/j.agrformet.2016.06.021

772 Mahl UH, Tank JL, Roley SS, Davis RT (2015) Two-stage ditch floodplains enhance N-removal  
773 capacity and reduce turbidity and dissolved P in agricultural streams. *JAWRA* 51(4):923–940. doi:  
774 10.1111/1752-1688.12340

775 Manners R, Wilcox AC, Kui L, Lightbody A, Stella J, Sklar L (2015) When do plants modify fluvial  
776 processes? Plant-hydraulic interactions under variable flow and sediment supply rates. *Water Resour*  
777 *Res* 120(2):325–345. doi:10.1002/2014JF003265

778 McGahey C, Samuels PG, Knight DW, O'Hare MT (2008) Estimating river flow capacity in practice. *J*  
779 *Flood Risk Manage* 1(1):23–33

780 Middelkoop H, Asselman NEM, 1998. Spatial variability of floodplain sedimentation at the event scale  
781 in the Rhine-Meuse Delta, the Netherlands. *Earth Surface Processes and Landforms* 23, 561-573

782 Naiman RJ, Décamps H (1997) The ecology of interfaces: Riparian zones. *Annu Rev Ecol Syst* 28:621–  
783 658

784 Nepf H (2012) Flow and transport in regions with aquatic vegetation. *Annu Rev Fluid Mech* 44:123–  
785 142. doi:10.1146/annurev-fluid-120710-101048

786 Nepf H, Ghisalberti M, White B, Murphy E (2007) Retention time and dispersion associated with  
787 submerged aquatic canopies. *Water Resour Res* 43, W04422, doi:10.1029/2006WR005362

788 Niklas KJ (1997) Size- and age-dependent variation in the properties of sap- and heartwood in Black  
789 Locust (*Robinia pseudoacacia* L.). *Annal Bot* 79:473–478

790 O'Hare M (2015) Aquatic vegetation – a primer for hydrodynamic specialists. *J Hydraul Res* 53(6):687-  
791 698. doi:10.1080/00221686.2015.1090493

792 Osterkamp WR, Hupp CR, Stoffel M (2012) The interactions between vegetation and erosion: new  
793 directions for research at the interface of ecology and geomorphology. *Earth Surf Process Landforms*  
794 37:23–36. doi:10.1002/esp.2173

795 Owens PN, Batalla RJ, Collins AJ, Gomez B, Hicks DM, Horowitz AJ, Kondolf GM, Marden M, Page  
796 MJ, Peacock DH, Petticrew EL, Salomons W, Trustrum NA (2005) Fine-grained sediment in river  
797 systems: environmental significance and management issues. *River Res Applic* 21:693–717.  
798 doi:10.1002/rra.878

799 Pasquale N, Perona P, Francis R, Burlando P (2014) Above-ground and below-ground *Salix* dynamics  
800 in response to river processes. *Hydrol Process* 28:5189–5203. doi:10.1002/hyp.9993

801 Peltola HM (2006) Mechanical stability of trees under static loads. *Am J Bot* 93(10):1501–1511

802 Peralta G, van Duren LA, Morris EP, Bouma TJ (2008) Consequences of shoot density and stiffness for  
803 ecosystem engineering by benthic macrophytes in flow dominated areas: a hydrodynamic flume  
804 study. *Mar Ecol Prog Ser* 368:103–115. doi: 10.3354/meps07574

805 Powell GE, Ward AD, Mecklenburg DE, Draper J, Word W (2007) Two-stage channel systems: Part 2,  
806 case studies. *J Soil Water Conserv* 62(4):286–296

807 Schuurman F, Marra WA, Kleinhans MG (2013) Physics-based modeling of large braided sand-bed  
808 rivers: Bar pattern formation, dynamics, and sensitivity. *J Geophys Res Earth Surf* 118:2509–2527.  
809 doi:10.1002/2013JF002896

810 Sellin RHJ, van Beesten DP (2004) Conveyance of a managed vegetated two-stage river channel. *Water*  
811 *Management* 157(1):21–33. doi:10.1680/wama.2004.157.1.21

812 Sharpe RG, James CS (2006) Deposition of sediment from suspension in emergent vegetation. *Water*  
813 *SA* 32(2):211–218

814 Shields Jr. FD, Coulton KG, Nepf H (2017) Representation of vegetation in two-dimensional

815 hydrodynamic models. *J Hydraul Eng*, 02517002. doi:10.1061/(ASCE)HY.1943-7900.0001320  
816 Shiono K, Muto Y (1998) Complex flow mechanisms in compound meandering channels with overbank  
817 flow. *J Fluid Mech* 376:221–261  
818 Solari L, van Oorschot M, Belletti B, Hendriks D, Rinaldi M, Vargas-Luna A (2016) Advances on  
819 modeling riparian vegetation–hydromorphology interactions. *River Res Applic* 32:164–178. doi:  
820 10.1002/rra.2910  
821 Studer R, Zeh H (2014) Soil bioengineering - construction type manual. Verein für Ingenieurbioogie,  
822 European Federation for Soil Bioengineering. vdf Hochschulverlag AG der ETH Zürich,  
823 Switzerland. 440 pp. ISBN 978-3-7281-3642-8. [Open access, [http://vdf-online.ch/soil-](http://vdf-online.ch/soil-bioengineering/)  
824 [bioengineering/](http://vdf-online.ch/soil-bioengineering/)]  
825 Sukhodolov AN, Sukhodolova TA (2012) Vegetated mixing layer around a finite-size patch of  
826 submerged plants: Part 2. Turbulence statistics and structures. *Water Resour Res* 48:W12506.  
827 doi:10.1029/2011WR011805  
828 Thonon I, Roberti JR, Middelkoop H., van der Perk M., Burrough PA (2005) In situ measurements of  
829 sediment settling characteristics in floodplains using a LISST-ST. *Earth Surf Process Landforms* 30:  
830 1327–1343. doi:10.1002/esp.1239  
831 Thornton CI, Abt SR, Clary WP (1997) Vegetation influence on small stream siltation. *J Am Water*  
832 *Resour As* 33(6):1279–1288  
833 USDA (2007) Two-Stage Channel Design. In *National Engineering Handbook, Part 654, Stream*  
834 *Restoration Design*. United States Department of Agriculture, Natural Resources Conservation  
835 Service  
836 Uusitalo R, Yli-Halla M, Turtola E (2000) Suspended soil as a source of potentially bioavailable  
837 phosphorus in surface runoff waters from clay soils. *Water Res* 34(9):2477–2482  
838 Vargas-Luna A, Crosato A, Calvani G, Uijttewaal WSJ (2015a) Representing plants as rigid cylinders  
839 in experiments and models. *Adv Water Resour* 93(B):205–222. doi:  
840 10.1016/j.advwatres.2015.10.004  
841 Vargas-Luna A, Crosato A, Uijttewaal WSJ (2015b) Effects of vegetation on flow and sediment  
842 transport: comparative analyses and validation of predicting models. *Earth Surf Process Landforms*  
843 40:157–176. doi:10.1002/esp.3633  
844 Villada Arroyave JA, Crosato A (2010) Effects of river floodplain lowering and vegetation cover. *Water*  
845 *Management WM9*:457–467. doi: 10.1680/wama.900023  
846 Vogel S (1994) *Life in moving fluids – The physical biology of flow*, 2<sup>nd</sup> edition. Princeton University  
847 Press, Princeton  
848 Västilä K (2015) *Flow–plant–sediment interactions: Vegetative resistance modeling and cohesive*  
849 *sediment processes*. Doctoral thesis, Aalto University School of Engineering, Espoo, Finland.  
850 <http://urn.fi/URN:ISBN:978-952-60-6597-7>

851 Västilä K, Järvelä J (2011) Environmentally preferable two-stage drainage channels: considerations for  
852 cohesive sediments and conveyance. *Int J River Basin Manage* 9(3–4):171–180. doi:  
853 10.1080/15715124.2011.572888

854 Västilä K, Järvelä J (2014) Modeling the flow resistance of woody vegetation using physically-based  
855 properties of the foliage and stem. *Water Resour Res* 50(1):229–245. doi: 10.1002/2013WR013819

856 Västilä K, Järvelä J, Aberle J (2013) Characteristic reference areas for estimating flow resistance of  
857 natural foliated vegetation. *J Hydrol* 492:49–60. doi: 10.1016/j.jhydrol.2013.04.015

858 Västilä K, Järvelä J, Jalonen J (2015) Effect of floodplain vegetation on flow and transport of cohesive  
859 particles in an environmental two-stage channel. In *Proceedings, 36th IAHR World Congress, 28.6.–*  
860 *3.7.2015, Delft – The Hague, the Netherlands*

861 Västilä K, Järvelä J, Koivusalo H (2016) Flow–vegetation–sediment interaction in a cohesive compound  
862 channel. *J Hydraul Eng* 142(1): 04015034. doi:10.1061/(ASCE)HY.1943-7900.0001058

863 Whittaker P, Wilson C, Aberle J (2015) An improved Cauchy number approach for predicting the drag  
864 and reconfiguration of flexible vegetation. *Adv Water Res* 83:28–35. doi:  
865 10.1016/j.advwatres.2015.05.005

866 Wood PJ, Armitage PD (1997) Biological effects of fine sediment in the lotic environment. *Environ*  
867 *Manage* 21(2):203–217

868 Xavier P (2009) Floodplain woodland hydrodynamics. Doctoral thesis, Cardiff School of Engineering,  
869 Cardiff University, Cardiff, UK

870 Zinke P (2011) Modelling of flow and levee depositions in a freshwater delta with natural vegetation.  
871 Doctoral thesis. Faculty of Civil Engineering, Norwegian University of Science and Technology

872 Zinke P, Olsen NRB, Bogen J (2011) Three-dimensional numerical modelling of levee depositions in a  
873 Scandinavian freshwater delta. *Geomorphology* 129:320–333. doi:10.1016/j.geomorph.2011.02.027

874 Zong L, Nepf H (2011) Spatial distribution of deposition within a patch of vegetation. *Water Resour*  
875 *Res* 47:W03516. doi:10.1029/2010WR009516

876 Zou J, Yan G, Zhu L, Zhang W (2009) Woody-to-total area ratio determination with a multispectral  
877 canopy imager. *Tree Physiol* 29:1069–1080. doi:10.1093/treephys/tpp042

878

879

880 **Table 1** Summary of different formulations used to describe vegetative flow resistance

Formulation	Equation	Common usage
Drag force, $F$ [N]	Eq. 2	$F$ characterizes the drag forces exerted by plants under flow and is commonly applied in experimental investigations
Drag-density parameter, $C_{Da}$ [ $\text{m}^2 \text{m}^{-3}$ ]	Eq. 3	$C_{Da}$ describes the vegetative drag per unit water volume and is used as a sink or source term in 3D models; closely related to $F$
Drag-area parameter, $C_{Da}H$ [ $\text{m}^3 \text{m}^{-3}$ ]	Eq. 4	$C_{Da}H$ is used to characterize the bulk drag of submerged vegetation in approaches that have separate vertical layers for vegetation and overflow; closely related to $F$
Vegetative friction factor, $f''$ [-]	Eq. 5	$f''$ is used to represent the plant-stand scale flow resistance in flume studies and to describe roughness in 2D depth-averaged models
Vegetative Manning coefficient, $n_{\text{veg}}$ [-]	Eq. 6	Manning coefficient is widely used to describe reach-scale flow resistance in practical applications and 1D models, or roughness in 2D depth-averaged models

881

882 **Table 2** Parameter values for the use of Eqs. 2–6 ( $u_{\chi,F} = u_{\chi,S} = 0.2 \text{ m s}^{-1}$ ). Velocities up to  $0.8 \text{ m s}^{-1}$  were used in  
883 deriving the values

Species	$C_{D\chi,F}$	$\chi^F$	$C_{D\chi,S}$	$\chi^S$	Data source
<i>Alnus glutinosa</i> (Common Alder)	0.18	-1.11	0.89	-0.27	Västilä and Järvelä (2014)
<i>Betula pendula</i> (Silver Birch)	0.20	-1.06	1.02	-0.32	Västilä and Järvelä (2014)
<i>Betula pubescens</i> (White Birch)	0.10	-1.09	0.82	-0.25	Jalonen and Järvelä (2014)
<i>Populus nigra</i> (Black Poplar)	0.13	-0.97	0.95	-0.27	Västilä and Järvelä (2014)
<i>Salix alba</i> × <i>Salix fragilis</i> (hybrid Crack Willow)	0.19	-1.21	0.96	-0.25	Västilä and Järvelä (2014)
<i>Salix caprea</i> (Goat Willow)	0.09	-1.09	0.84	-0.27	Jalonen and Järvelä (2014)
<i>Salix viminalis</i> (Common Osier)	0.11	-1.21	1.03	-0.20	Västilä and Järvelä (2014)
Species-averaged	0.14	-1.11	0.93	-0.26	

884

885

886

887

Table 3. Factors representing vegetation and sediment properties to explain net deposition within floodplain vegetation (statistical significance from the present field data).

Explanatory factor	Effect on net deposition	Statistical significance
Cross-sectional vegetative blockage factor ( $B_\chi$ )	+	Highly significant ***
Flow velocity within vegetation ( $u_v$ )	-	Significant **
Distance from sediment supply point ( $x_s$ )	-	Significant **
Suspended sediment load	+	Not evaluated/see text
Settling velocity ( $w_s$ )	+	Not evaluated/see text

888 \*\*\*  $p \leq 0.001$ ; \*\*  $p \leq 0.01$

889

890 **Figure captions**

891

892 **Fig 1** Determination of the cross-sectional vegetative blockage factor and interfaces  $L_b$  and  $L_v$  of Eqs. 7–8

893 **Fig 2** Effect of vegetation on the turbulent flow structure and sediment transport in sparse plant stands (a) and  
894 dense plant stands (b), with the density limits ( $C_{Da}H$ ) according to Nepf (2012). Patterns #1–#2 relate to turbulence  
895 generated by individual plants (#1) and by stand-scale shear layers (#2) [modified from Västilä (2015)]

896 **Fig 3** The field site with the constructed floodplain (a), and a representative cross-section with the measured mean  
897 annual net deposition (b)

898 **Fig 4** The test reach with the five differently vegetated sub-reaches, including the locations of main monitoring  
899 activities.

900 **Fig 5** Mean drag forces of leafless and foliated, 0.9–3.1 m tall woody plants (Xavier 2009; Jalonen and Järvelä  
901 2014) (a), and mean errors in the drag forces predicted with Equation 2 (b)

902 **Fig 6** Usage of the flow resistance parameterization (Eqs. 2–6) in plant-scale, plant stand-scale, and reach-scale  
903 analyses at different relative submergences ( $h/H$ ). The recommended characteristic approach velocities ( $u_c$ ) are  
904 shown, with  $u_v$  denoting the mean velocity in the vegetated part of the cross-section. Equations are written for the  
905 drag force ( $F$ ), vegetative friction factor ( $f''$ ), drag–density parameter ( $C_{Da}$ ), drag–area parameter ( $C_{Da}H$ ) and  
906 vegetative Manning coefficient ( $n_{veg}$ ) using the one-sided leaf area ( $A_L$ ), frontal projected stem area ( $A_S$ ), unit bed  
907 area ( $A_B$ ), the leaf area per unit volume ( $a_L$ ) and the stem area per unit volume ( $a_S$ ). Values of  $\chi_F$ ,  $\chi_S$ ,  $C_{D\chi,F}$ ,  $C_{D\chi,S}$ ,  
908  $u_{\chi,F}$ , and  $u_{\chi,S}$  are reported in Table 2 for common riparian species. Note that all vegetative reference areas refer to  
909 the wet parts of the plants

910 **Fig 7** Work-flow for estimating vegetative flow resistance using Eqs. 2–6 (Fig. 6)

911 **Fig 8** The modelled (Eqs. 7–8) bulk mean velocities within and above floodplain vegetation at different flow  
912 events. For submerged conditions, the discontinuity at the top of the vegetation (marked with a dashed line) is due  
913 to the two-layer representation in Eqs. 7–8.

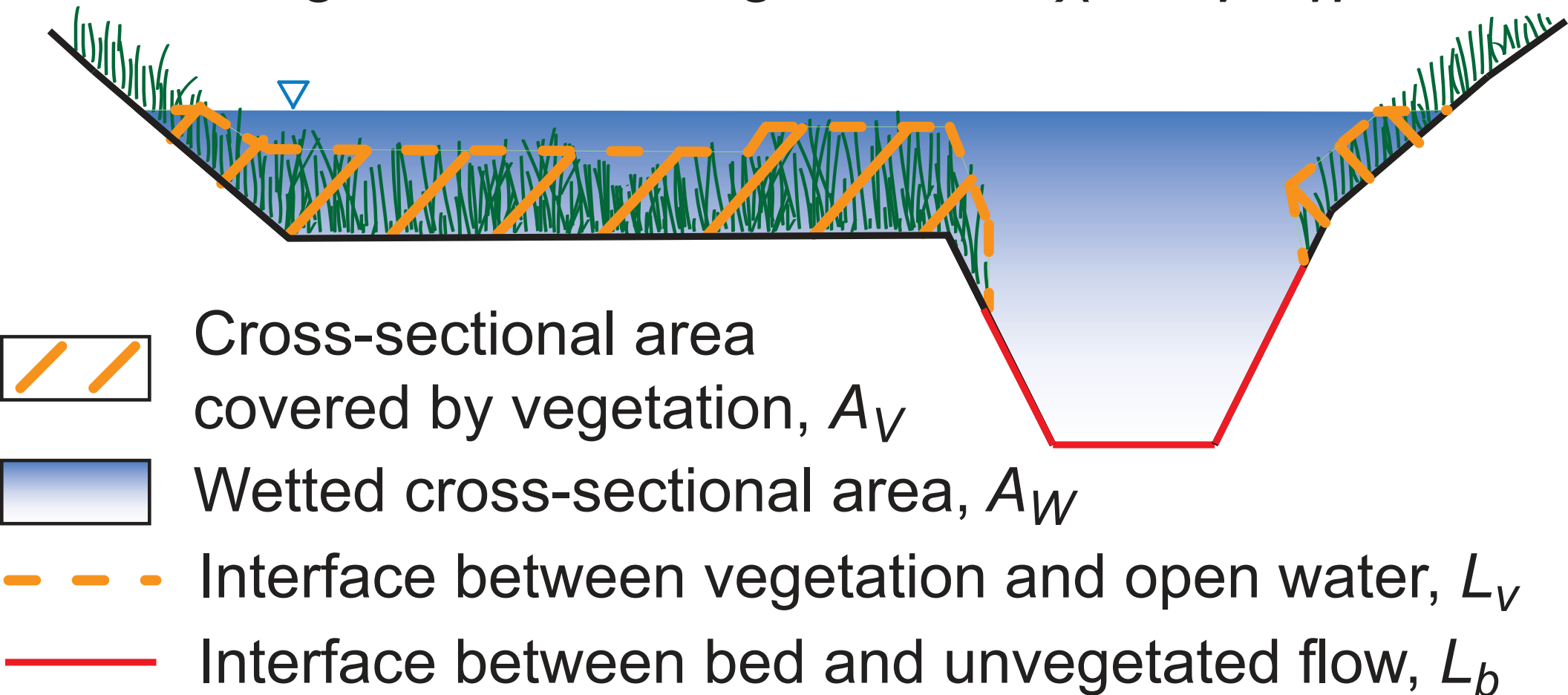
914 **Fig 9** The modelled (Eqs. 7–8) discharges on the floodplain at different floodplain water depths. The discharge  
915 increased more rapidly after vegetation became submerged (as illustrated by the changes in the slopes of the curves  
916 for Grasses-U and -D at water depths equaling vegetation height, i.e., ~0.26 m and 0.36 m, respectively).  
917 Vegetation in Grasses-N and Willows-M was emergent and in Bare-M fully submerged at all modelled water  
918 depths.

919 **Fig 10** Net deposition as measured (mean values for the ten cross-sections with the bars showing  $\pm 1$  standard error,  
920  $N=200$ ) and estimated by the multiple regression; also the two-year mean vegetation heights and dry masses are  
921 shown. The diagonal line denotes the perfect fit. The explanatory factors of the model were the cross-sectional  
922 vegetative blockage factor, distance from the sediment supply point, and the flow velocity within the vegetation.

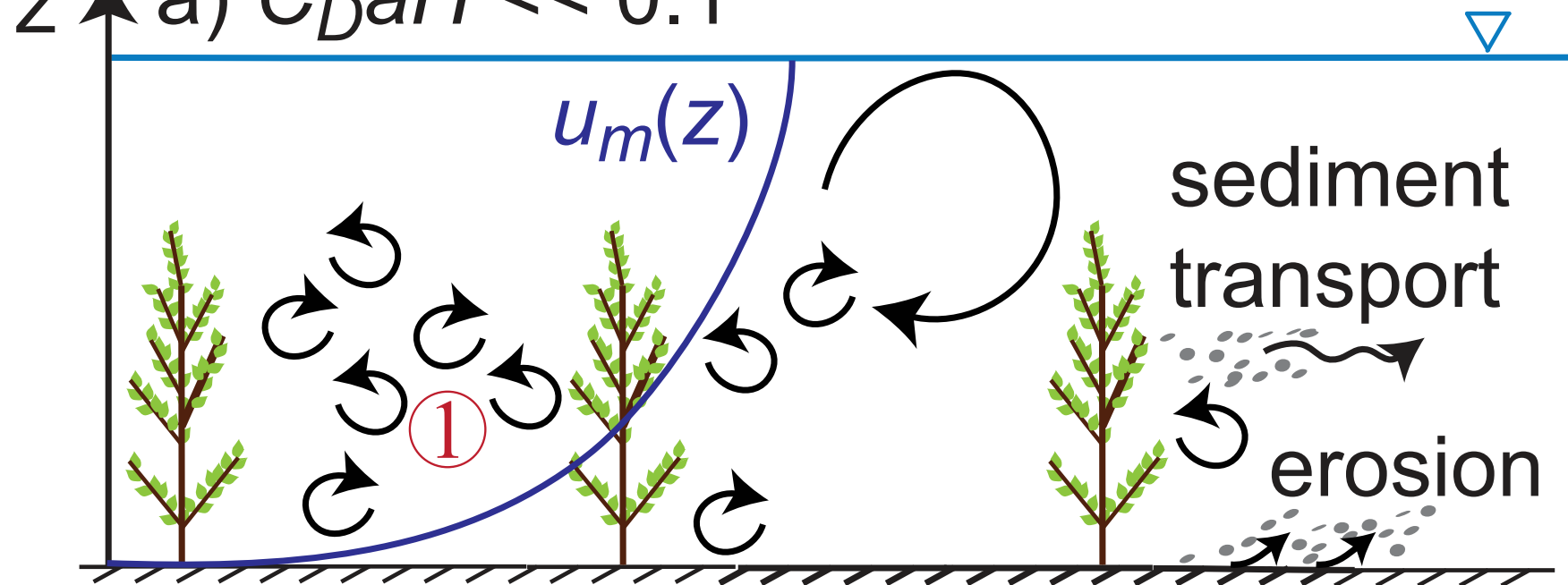
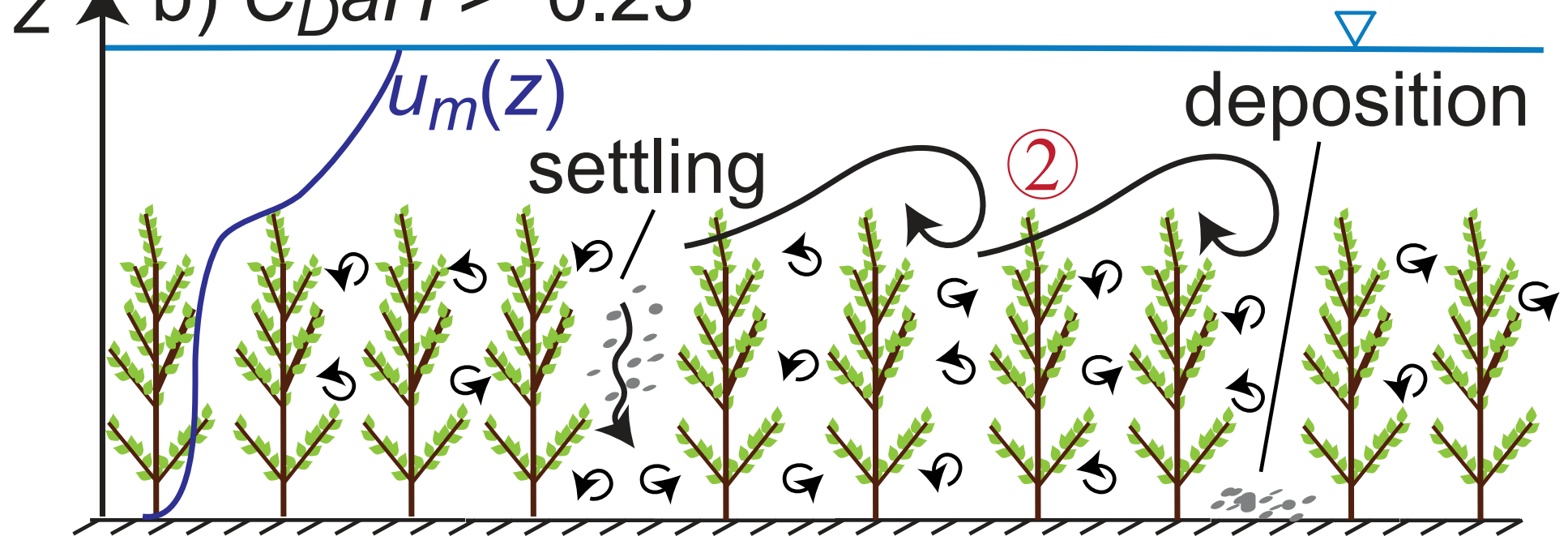
923 **Fig 11** Particle size distribution of the dispersed, deposited sediment in two sub-reaches determined by laser  
924 diffraction and hydrometer methods (bars showing  $\pm 1$  standard error,  $N=3-5$ ).

925 **Fig 12** Annual suspended sediment mass balance in the 190 m long compound test reach with the estimated specific  
926 loads from fields ( $40 \text{ t km}^{-2} \text{ a}^{-1}$ ) and forests ( $7 \text{ t km}^{-2} \text{ a}^{-1}$ ). Overbank flows conveyed 89% of the incoming sediment  
927 load while 5.5% of the total annual load was deposited on the floodplain

Vegetative blockage factor  $B_X = A_V/A_W$



→ flow direction

z ↑ a)  $C_D aH \ll 0.1$ z ↑ b)  $C_D aH > \sim 0.23$ 



a)



b)

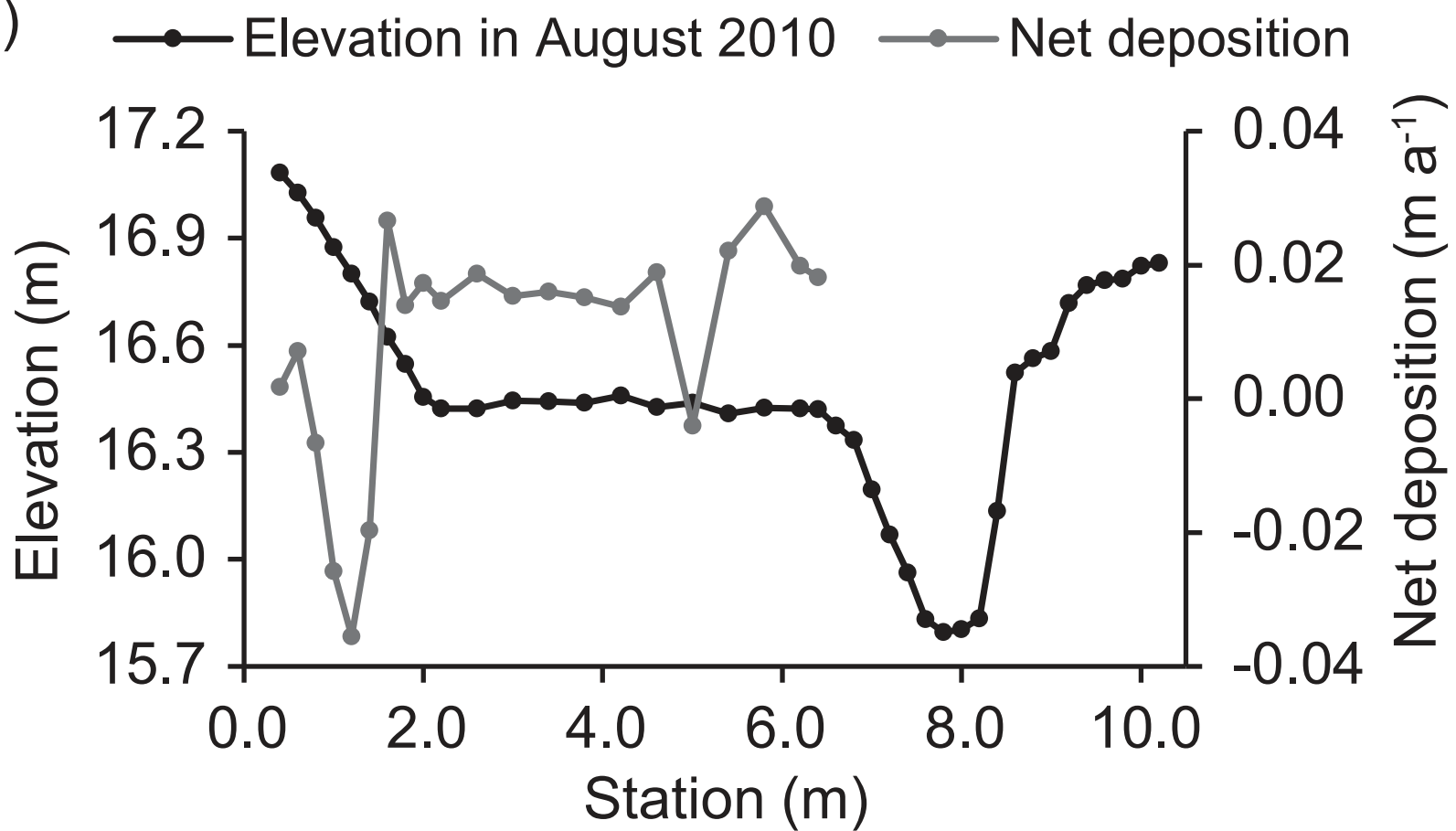


Fig4

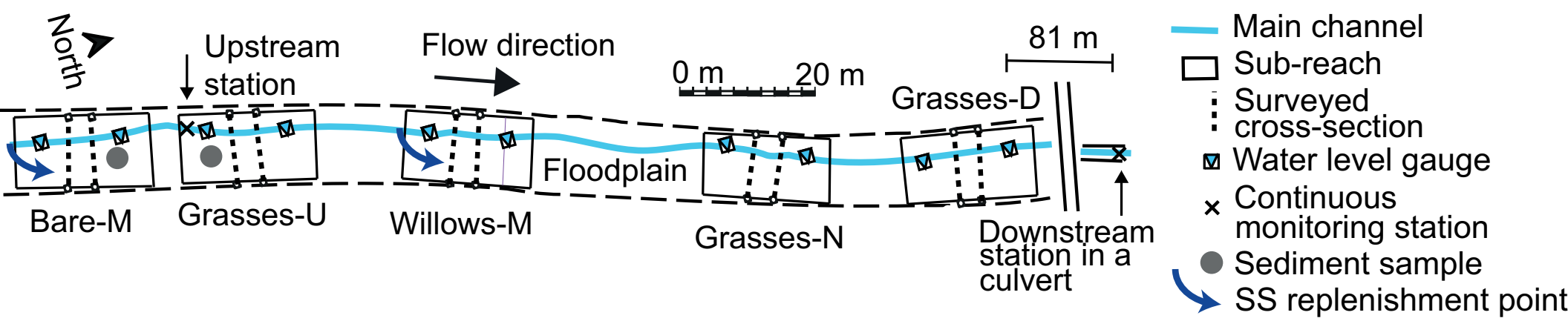
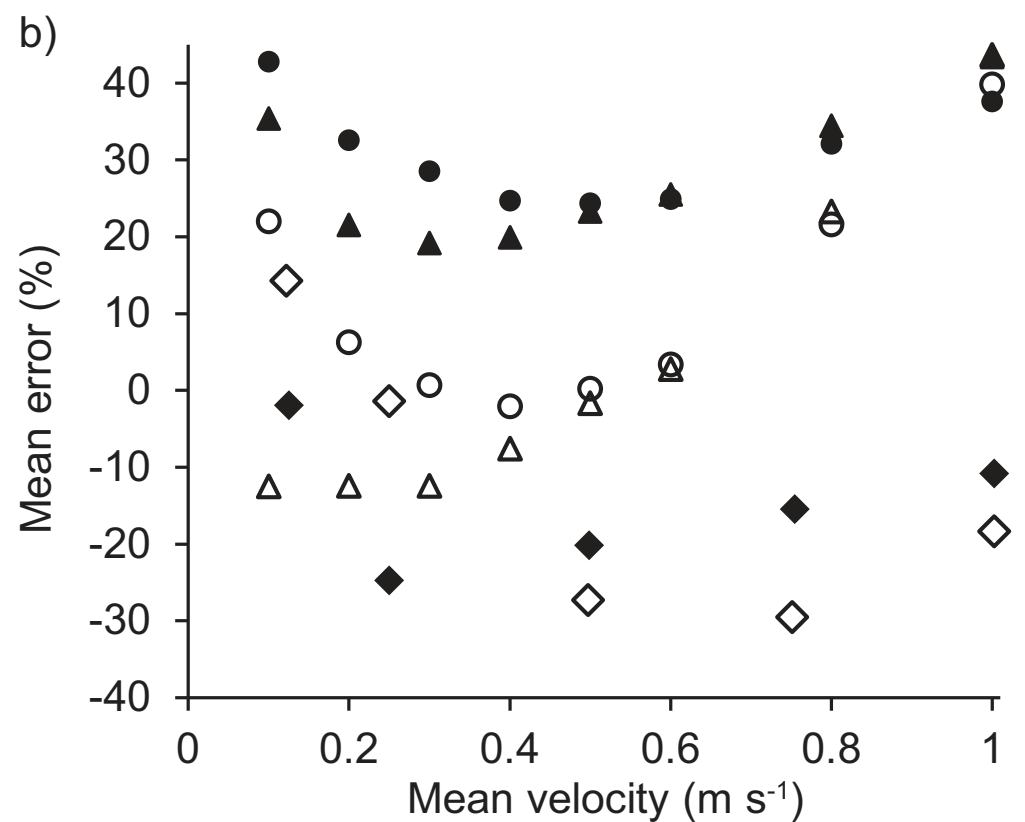
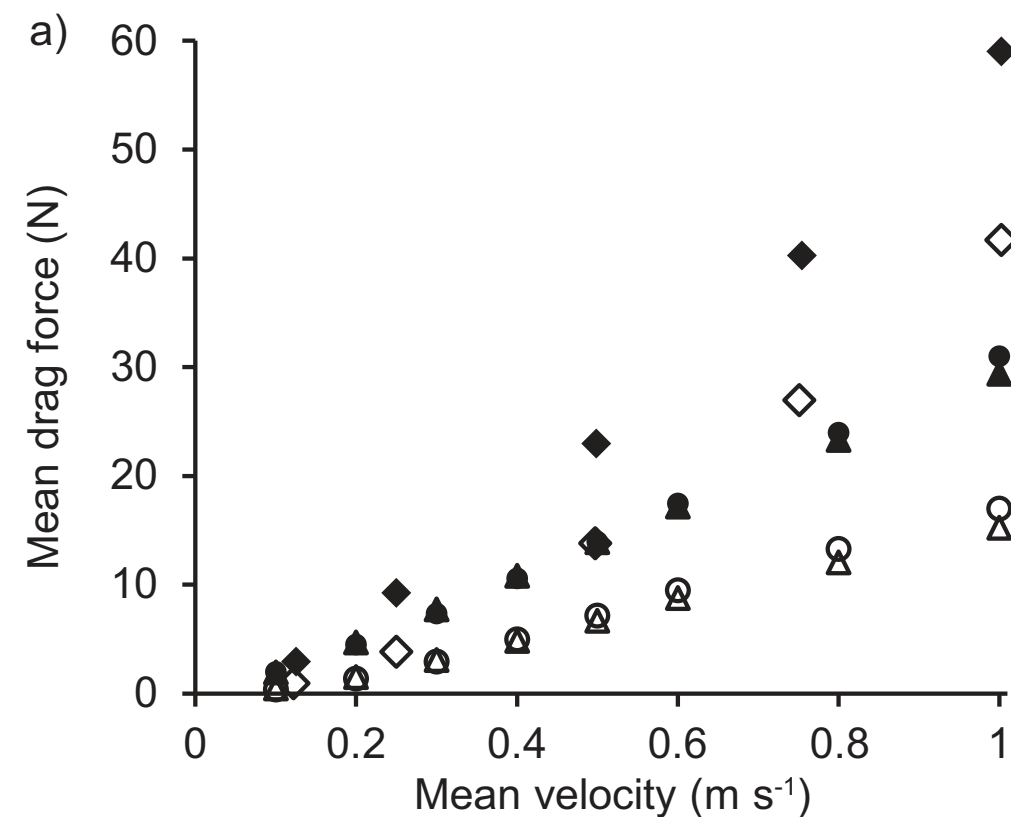


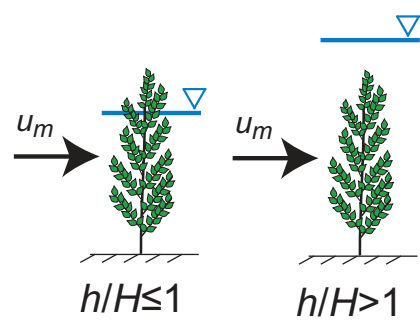
Fig5

- *A. glutinosa*, foliated (Jalonen & Järvelä 2014)
- ▲ *B. pendula*, foliated (Jalonen & Järvelä 2014)
- ◆ *A. glutinosa*, foliated (Xavier 2009)

- *A. glutinosa*, leafless (Jalonen & Järvelä 2014)
- △ *B. pendula*, leafless (Jalonen & Järvelä 2014)
- ◇ *A. glutinosa*, leafless (Xavier 2009)



### a) Plant scale

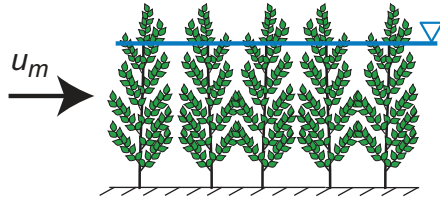


For both  $h/H \leq 1$  and  $h/H > 1$ , use depth-averaged mean velocity as  $u_C$  with:

$$F = \frac{1}{2} \rho \left[ C_{D\chi,F} \left( \frac{u_C}{u_{\chi,F}} \right)^{\chi_F} A_L + C_{D\chi,S} \left( \frac{u_C}{u_{\chi,S}} \right)^{\chi_S} A_S \right] u_C^2 \quad (\text{Eq. 2})$$

### b) Plant stand scale (fully developed flow)

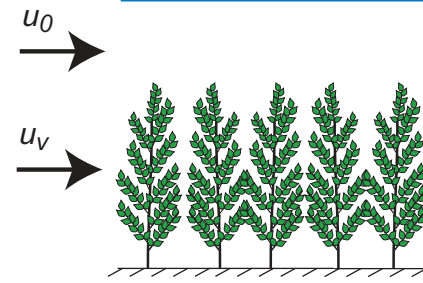
$h/H \leq 1$



For  $h/H \leq 1$ ,  
use mean velocity  
as  $u_C$  with:

$$f'' = 4 \left[ C_{D\chi,F} \left( \frac{u_C}{u_{\chi,F}} \right)^{\chi_F} \frac{A_L}{A_B} + C_{D\chi,S} \left( \frac{u_C}{u_{\chi,S}} \right)^{\chi_S} \frac{A_S}{A_B} \right] \quad (\text{Eq. 5})$$

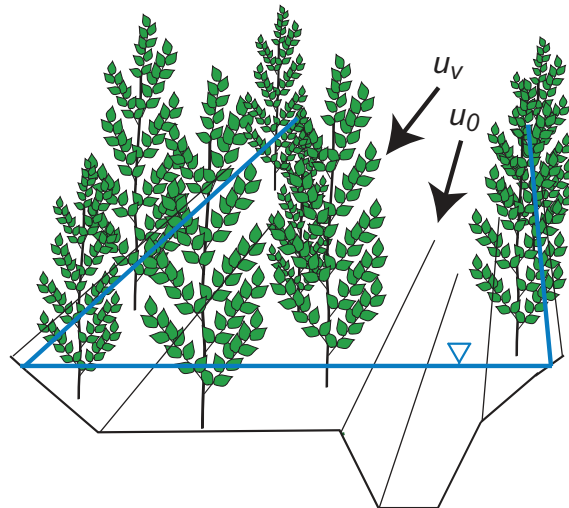
$h/H > 1$



For  $h/H > 1$ ,  
use  $u_C = u_v$  and  
replace the  
 $C_{D\chi} a H$   
parameter with:

$$C_{D\chi} a H = C_{D\chi,F} \left( \frac{u_C}{u_{\chi,F}} \right)^{\chi_F} \frac{A_L}{A_B} + C_{D\chi,S} \left( \frac{u_C}{u_{\chi,S}} \right)^{\chi_S} \frac{A_S}{A_B} \quad (\text{Eq. 4})$$

### c) Reach scale



Use  $u_C = u_v$  and replace the  $C_{D\chi} a$  parameter in analytical or numerical models with:

$$C_{D\chi} a = C_{D\chi,F} \left( \frac{u_C}{u_{\chi,F}} \right)^{\chi_F} a_L + C_{D\chi,S} \left( \frac{u_C}{u_{\chi,S}} \right)^{\chi_S} a_S \quad (\text{Eq. 3})$$

For practical applications in terms of Manning's  $n$  with  $K=1 \text{ m}^{1/3} \text{ s}^{-1}$ :

$$n_{veg} = \frac{Kh^{1/6}}{\sqrt{2g}} \sqrt{C_{D\chi,F} \left( \frac{u_C}{u_{\chi,F}} \right)^{\chi_F} \frac{A_L}{A_B} + C_{D\chi,S} \left( \frac{u_C}{u_{\chi,S}} \right)^{\chi_S} \frac{A_S}{A_B}} \quad (\text{Eq. 6})$$

Select a resistance formulation suitable for the case (see Table 1)

- Equations 2–6 in Figure 6 for  $F$ ;  $C_{Da}$ ;  $C_{Da}H$ ;  $f'$ ;  $n_{veg}$

Determine the vegetative reference areas per ground area ( $A_L$ ;  $A_s$ ) or water volume ( $a_L$ ;  $a_s$ )

- Literature data
- Laser scanning
- Photographic methods
- Manual sampling

Determine drag coefficients ( $C_{D\chi,F}$ ;  $C_{D\chi,S}$ ) and reconfiguration parameters ( $\chi_F$ ;  $\chi_S$ ) which are constant for the selected range of characteristic velocity  $u_c$

- Literature (see e.g. Table 2)
- Experimentally using values  $\sim 0.05$ – $0.2 \text{ m s}^{-1}$  for the scaling velocities  $u_{\chi,F}$  and  $u_{\chi,S}$  (see section 4.2)

Determine  $u_c$  (e.g. depth-averaged mean velocity or mean velocity in the vegetated part of the cross-section; Figure 6)

- Iteratively from hydraulic computations or models (1/2/3D)
- Experimentally: velocity measurements in the field or laboratory

Compute the flow resistance value noting that iteration is needed, as the resistance and velocity are interconnected

- Equations 2–6 (see Figure 6)

Use computed  $F$ ;  $C_{Da}$ ;  $C_{Da}H$ ;  $f'$  or  $n_{veg}$  as input in hydraulic and morphological models

Fig8

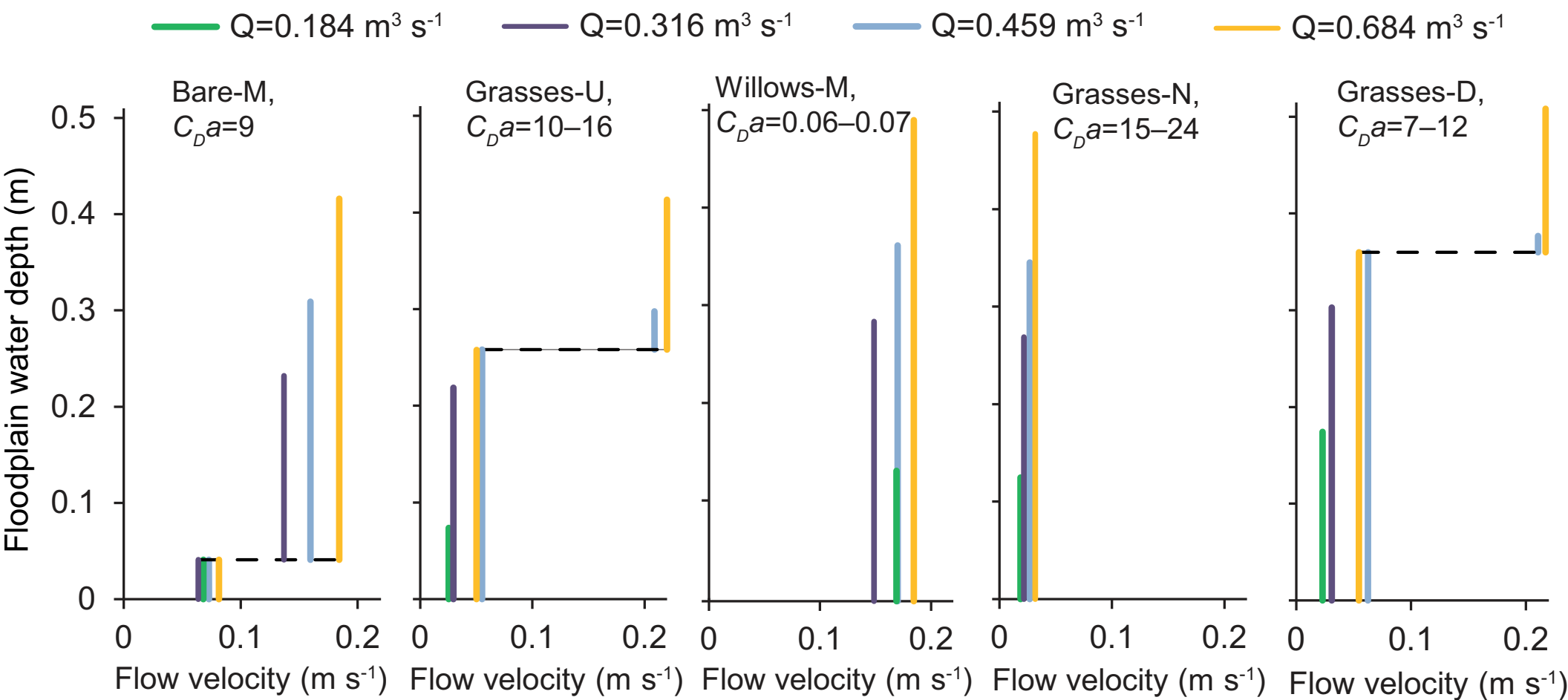


Fig9

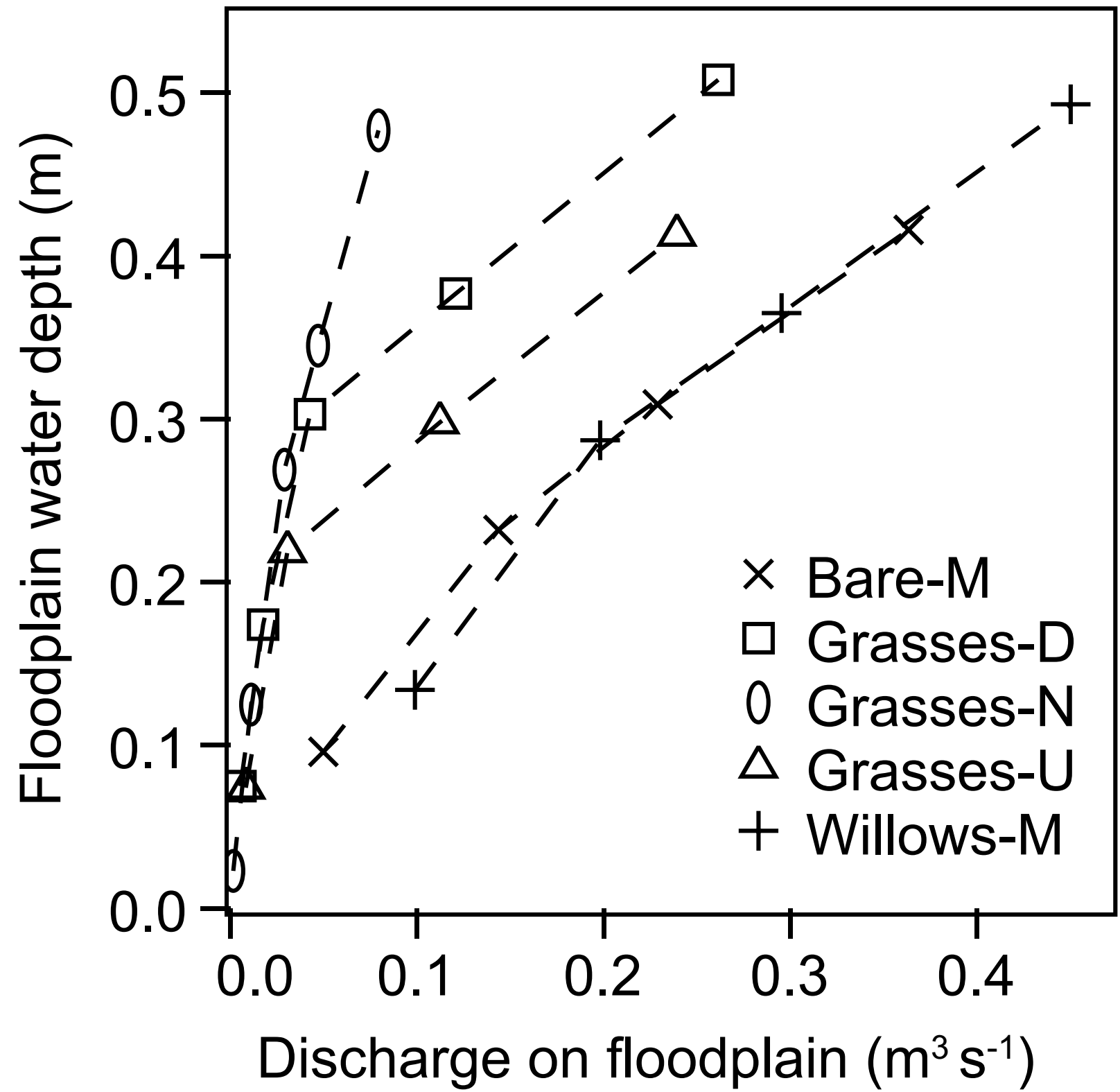


Fig10

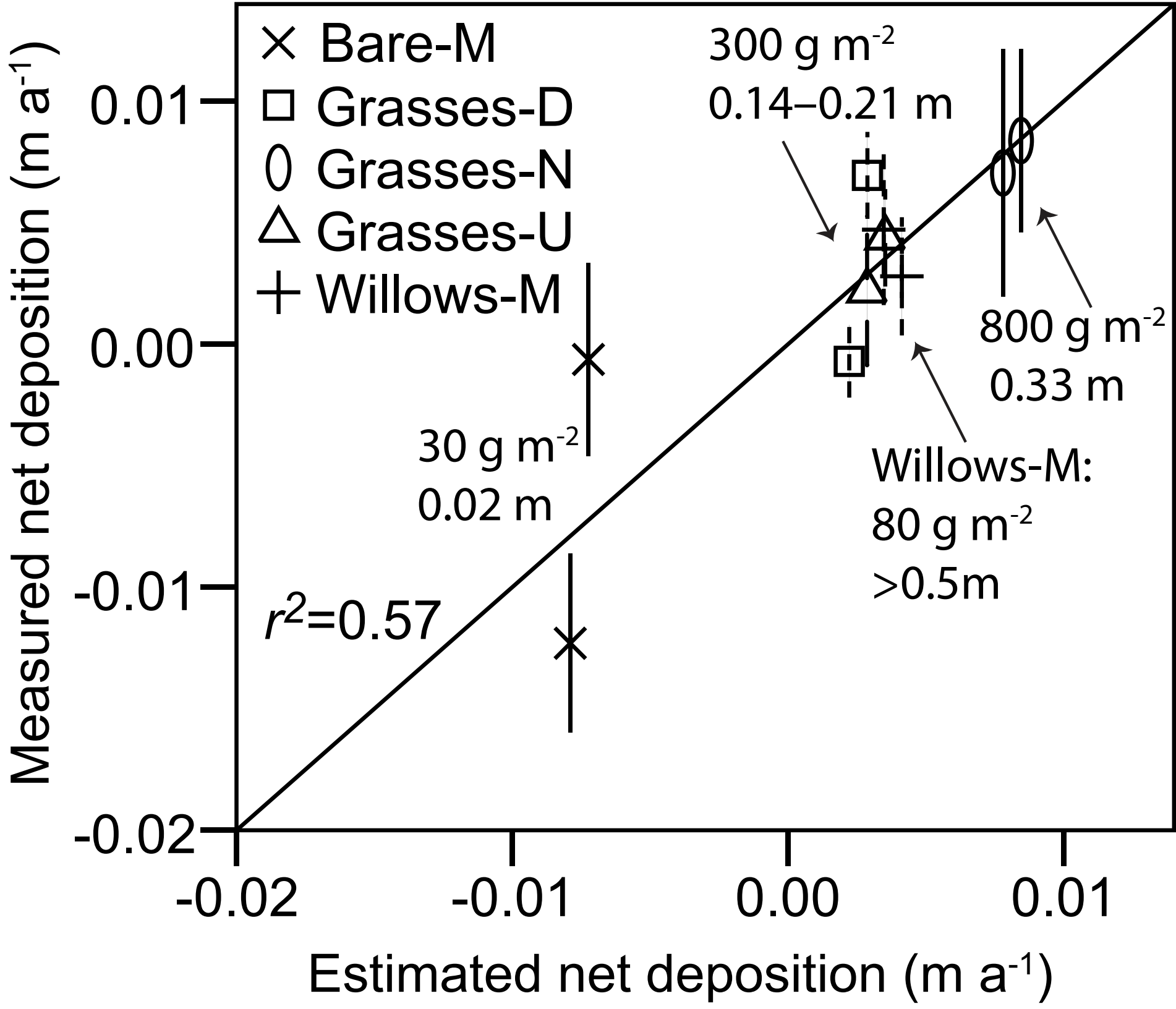




Fig11

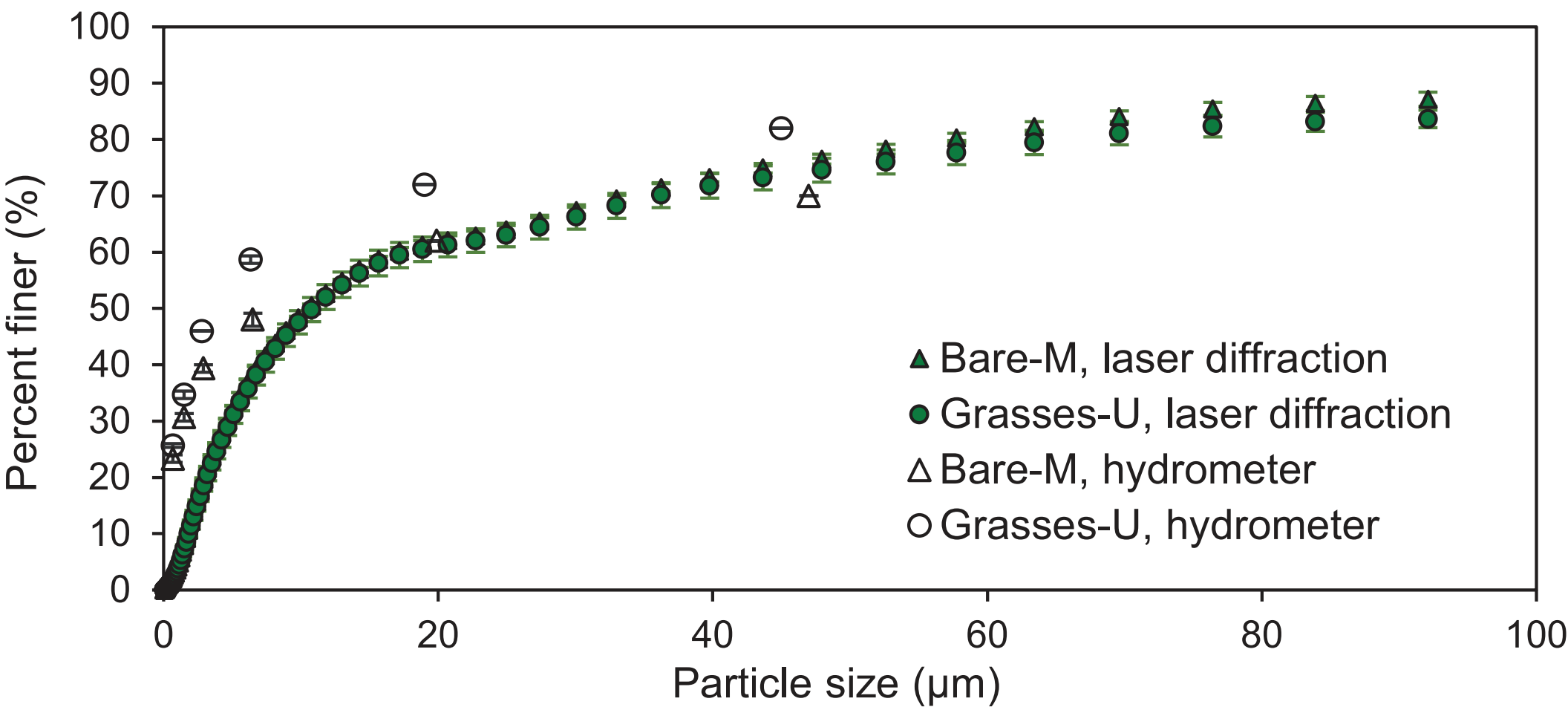


Fig12

